Recent advances in microscale extraction driven by ion concentration polarization

Aparna Krishnamurthy, Robbyn K. Anand*

Department of Chemistry, Iowa State University, 1605 Gilman Hall, 2415 Osborn Drive, Ames, IA 50011, USA

*To whom correspondence should be addressed, *rkanand@iastate.edu*

Article information

Keywords: ion concentration polarization, faradaic, extraction, separation, microfluidics, membrane, permselective, preconcentration

Abbreviations

ICP, ion concentration polarization; fICP, faradaic ion concentration polarization, EDL, electrical double layer; EOF, electroosmotic flow; DEP, dielectrophoresis; AEM, anion exchange membrane; CEM, cation exchange membrane; BGE, background electrolyte; PDF, pressure-driven flow; ITP, isotachophoresis; IEF, isoelectric focusing; EFGF, electric field gradient focusing; ICPF, ion concentration polarization focusing; FF-ICP, free flow ion concentration polarization; BDP, BODIPY™ disulfonate; AF647, Alexa Fluor™ 647 carboxylic acid, tris(triethylammonium) salt; CB, Cascade Blue™ hydrazide trisodium salt; μPAD, microfluidic paper-based analytical device; CMC, critical micelle concentration; HOLMES, hierarchical nanofluidic molecular enrichment system; CP, concentration polarization; LSV, linear sweep voltammetry; EV, extracellular vesicles; PS, polystyrene; EFG, electric field gradient

Contents

Abstract

Microscale extraction offers several distinct advantages over bench-scale processes including increases in sample throughput, specificity, and efficiency. These attributes can be harnessed to improve the efficacy of assays, amplify analyte signals in sensors or purify samples. Recently, electrokinetic microextraction techniques have garnered increased attention owing to advantages such as control over mass transport, ease of actuation, and portability, which allow them to be readily incorporated into microscale and point-of-care devices. Ion concentration polarization (ICP) continuously creates an electric field gradient that can drive electrokinetic focusing. While the majority of articles on ICP have deliberated on analyte preconcentration, very few have ventured the subsequent extraction step – separation into another phase. The overarching aim of this review is to discuss recent developments in microfluidic extraction methods facilitated by ICP and the potential for their further advancement. Fundamental strategies used to achieve ICP-mediated extraction of distinct classes of analytes are discussed.

1. Introduction

Extraction is the spatiotemporal separation of analytes of interest from one phase comprising the sample into or onto another phase – a liquid or solid extract. In microextraction, the interface over which extraction occurs has a critical dimension on the order of several to hundreds of microns. For example, solid phase microextraction (SPME) utilizes a microscale fiber to separate analytes from sample volumes ranging from about one hundred microliters to several milliliters. For this reason, microextraction confers distinct advantages such as rapid processing of samples and minimal reagent consumption. In the context of microfluidics, both sample and extraction phases are on the pico- to microliter scale. Further, the surface-to-volume ratio is relatively higher than that at the macroscale. These features can be leveraged to provide control over mass transport and to yield exhaustive extraction where motivated by the application.

Microfluidic length scales enhance mass transport by facilitating electrokinetic control over fluid flow by electroosmosis and the distribution of charged analytes by electromigration, which in the context of extraction, confers selectivity. In 2016, a review by Wuethrich et al. discussed the advantages of electric field-based methods and highlighted an increase in the adoption of these methods for separation in classical and microfluidic scales [1]. Various techniques used for electrokinetic preconcentration and/or extraction include dielectrophoresis (DEP) [2–5] and electric field gradient focusing techniques such as ion concentration polarization (ICP), bipolar electrode (BPE) focusing [6,7] isoelectric focusing (IEF), isotachophoresis (ITP) [8], on-chip electromembrane extraction (EME) [9] and bifurcated continuous field-flow fractionation (BCFFF) [10]. Further, these electrokinetic focusing and/or extraction strategies have been integrated with enzymatic assays [11], sensing [12–14], and cell analysis [15–17]. Implementation of electrokinetic methods has become increasingly straightforward as the integration of electrodes within microfluidic systems can be easily accomplished by approaches such as ink jet printing [18]. Moreover, a wide range of electrode materials such as Au, Pt, Cu, Ag, carbon, and stainless steel can be used to suit specific applications [19,20].

ICP is the simultaneous enrichment and depletion of ions at opposite ends of a nanochannel (or ion permselective membrane) connecting two microchannels, upon the application of a voltage bias across them. The generated ion depleted zone (IDZ) is highly resistive and leads to local enhancement of the electric field strength. An electric

field gradient at its boundary supports counter-flow focusing of charged species. An IDZ can similarly be generated by faradaic reactions occurring at an electrode embedded in a microfluidic device. Such faradaic ICP (fICP) employs charge transfer reactions to neutralize ions of the background electrolyte (BGE). Early studies to quantify ICP were carried out by Leinweber and Tallerek in a fixed bed of ion-permselective beads. They noticed highly chaotic flow patterns in the extraparticle bulk fluid and an immobile intraparticle space charge region [21]. fICP was first developed to enrich negatively charged analytes using a BPE in a straight microchannel [22]. Despite their relatively new emergence into the world of analytics, ICP and fICP techniques have revolutionized the area of analyte preconcentration and electrokinetic focusing. Preconcentration factors up to 10^6-fold in a single step have been achieved. The use of these two techniques for the purpose of extraction holds potential for high impact and broader applications in the fields of separation sciences, sensors, bioanalysis, and diagnostics. ICP-based techniques can confer unique advantages for the purpose of extraction such as on-demand extraction, successive or continuous extraction, regulated and selective mass transport, and tailored resolution (for example, stringent focusing by manipulation of counteracting convective and electrophoretic forces or use of electrophoretic spacers).

The current review highlights recent advancements in ICP/fICP-based microscale extraction and focuses on the interplay of intrinsic and extrinsic factors harnessed to achieve analyte separation. These factors include the charge carried by ionic analytes, the spatially averaged magnitude of the electric field and fluid velocity, the device architecture, and the properties of materials comprising microchannels, membranes and electrodes. At the outset, the mechanisms of ICP and fICP are introduced, followed by an evaluation of key features of these techniques in the context of extraction. Thereafter, recent advances in the extraction of distinct classes of analytes including atomic and polyatomic ions, smaller molecular ions, biopolymers, bioparticles, microbeads and microplastics are discussed with an emphasis on the distinct strategies used to achieve varied end goals such as ICP-based multitargeted extraction, analyte purification, and extraction-mediated sensing. Challenges to ICP-based microextractions spanning from separation resolution, quantification, efficiency, detection limits to bubble formation, have been addressed by some of the advances discussed in this review. In addition, potential opportunities in ICP-based microextractions to interface electrokinetic focusing with a range of orthogonal extraction strategies are discussed.

2. Mechanism of ICP

2.1. Generation of ion depleted and ion enriched zones

ICP is an electrokinetic phenomenon that is induced by the application of a voltage bias across an ion permselective junction resulting in the simultaneous, spatially distinct enrichment and depletion of ions. In the general case, a nanochannel bridges two microfluidic compartments (**Scheme 1a**) [23]. If the walls of the nanochannel are negatively charged (**Scheme 1b**), cations from the anodic compartment electromigrate across the nanochannel and into the cathodic compartment where they interact with anions converging at the junction. Anions in the anodic compartment migrate towards the driving electrodes, where a faradaic reaction (often water oxidation) occurs. The eventual movement of cations and anions away from the anodic micro-/nano- junction leads to the formation of an IDZ. At the cathodic end of the junction, accumulation of cations and anions leads to ion enriched zone (IEZ) formation.

2.2. Mechanisms of selective ion transport

The propagation of current in microscale compartments is facilitated by both cationic and anionic charge carriers, whereas in ion permselective junctions most (or all) of the current is carried by only one type of ion. This charge selection can be attributed to the exclusion of co-ions from electrical double layers (EDLs) formed along opposing walls

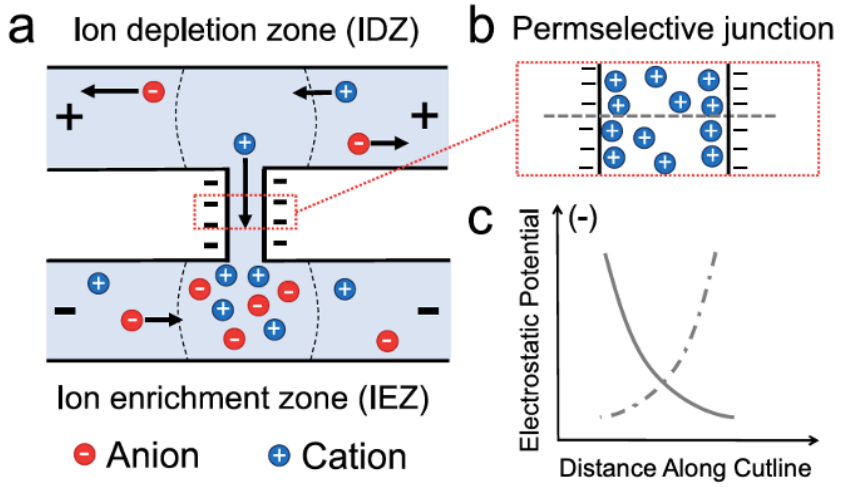

Scheme 1. Scheme illustrates a) IDZ and IEZ formation at opposite nanochannel-microchannel junctions; b) Cation occupying the overlapping electrical double layers (EDLs) from the two negatively charged nanochannel walls; and c) Profile of electrostatic potential from each nanochannel wall along the dashed line in (b). While depicted here, EDL overlap is not required for ion permselection. A modified version of the original illustration is reprinted with permission from ref [23].

of the nanochannel. Ion conduction through these EDLs is selective for counterions and can therefore lead to redistribution of charge carriers. For example, if the walls of the nanochannel or membrane are negatively charged, the entry of anions is restricted. The results of both experimental [24,25] and theoretical [26] studies have demonstrated that the deciding factor for the occurrence of concentration polarization is the dominance of surface conductance (through the EDLs) over bulk conductance. ICP has been observed across even microscale junctions under conditions of low electrolyte concentration and high surface charge, at which this requirement is met [24,25].

2.3. Local electric field gradient

When a voltage bias is applied between the inlet and outlet of a microchannel having a constant cross-sectional area and a homogeneous distribution of ions within the bulk solution, a uniform electric field results. In ICP, this electric field is perturbed by the differential conductance and alternate current paths associated with IDZ and IEZ formation. Since the IDZ is depleted of ions, there is a sharp decrease in conductance and therefore a drastic increase in solution resistance. In compliance with Ohm's and Kirchoff's laws, this resistance results in an enhanced electric field strength ($\vec{E} = -\nabla\emptyset$) within the IDZ. Thus, an electric field profile with localized high intensity is established. This electric field enhancement augments and redirects subsequent mass transport of ions leading to self-amplification of the local electric field strength, creating an extended space-charge region. The axial electric field component (along the length of the microchannel) peaks at the region of greatest ion depletion and tapers towards the edge or boundary of the zone, thus forming an extended electric field gradient [27]. To achieve analyte extraction, this gradient is exploited for counter-flow focusing, which is discussed in more detail in *Section 4.1*.

3. Mechanism of fICP

Faradaic ICP offers a similar effect of selective ion depletion and enrichment as does ICP, except that faradaic electrochemical processes (electron transfer reactions) drive these processes in contrast to ion permselection.

fICP techniques commonly employ a bipolar electrode (BPE), which is an electrode possessing a floating potential – the BPE is not in ohmic contact with the power supply. Oxidation and reduction of BGE ions can be facilitated at opposing ends

of the BPE upon application of a voltage bias (**Scheme 2b**). Reduction reactions such as neutralization of BGE cations into neutral species result in ion depletion at a BPE cathode. At the BPE anode, an oxidation reaction leading to generation of cations from neutral species may occur. This introduction of additional cations in turn attracts BGE anions, and therefore, enrichment of ions is observed at the anodic end. Equations 1-3 show redox reactions and subsequent neutralization of a buffer cation ($TrisH^+$) that results in BGE ion depletion and enrichment at the BPE cathode and anode, respectively (**Scheme 2d**):

At cathode: $2H_2O + 2e^- \rightarrow H_2 + 2OH^-$ (1)

$OH^- + TrisH^+ \rightarrow Tris + H_2O$ (2)

At anode: $2H_2O \rightarrow O_2 + 4H^+ + 4e^-$ (3)

It is important to note that as in ICP (**Scheme 2a**), the net effect of fICP (**Scheme 2b,d**) is apparent selective ion transport (**Scheme 2c**) [7]. **Scheme 2a** shows the ICP-driven selective mass transport of cations. Cations are transported across the nanochannel from the anodic to the cathodic microchannel compartments. In the case

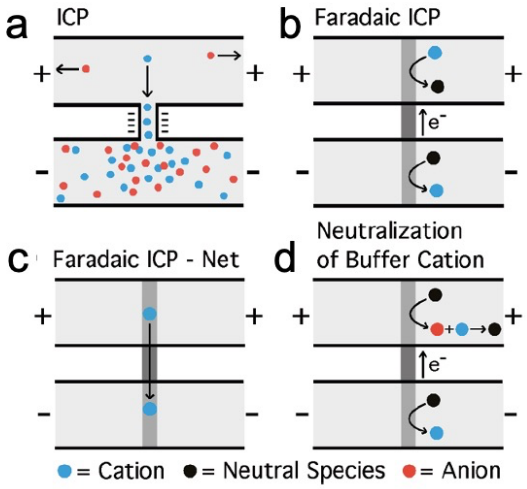

Scheme 2. Schematic illustration of a) selective transport of cations from the anodic to cathodic compartment across a nanochannel resulting in ICP; b) fICP arising from reduction of electrolyte cations into neutral species at the BPE cathode (anodic compartment) and oxidation of neutral species to cations at the BPE anode (cathodic compartment); c) net effect of fICP – selective transport of a cation across the junction is depicted; and d) alternate mechanism of IDZ development by a charge transfer reaction followed by neutralization of the BGE cation. Illustration is reprinted with permission from ref [7].

of fICP, buffer cations are 'depleted' from the anodic microchannel by their neutralization while being generated at the cathodic compartment (**Scheme 2b,d**). The depletion of buffer cations from one side of the nanochannel, and their generation at the

opposing side is analogous to cation transport across the nanochannel (**Scheme 2c**). Underlying mechanisms however differ in the sense that ICP is based on ion permselective mass transport and fICP on charge transfer reactions, which introduces a specie-dependent barrier to ion depletion – only those BGE ions that can be neutralized directly by a redox reaction or indirectly (e.g., by a following acid-base reaction) will be depleted. In a BGE comprising a mixture of buffer and salt ions, partial ion depletion is possible. For this reason, ICP is more versatile for application in a wide range of BGE compositions. On the other hand, systems have been devised to generate IDZs at both the BPE anode and cathode simultaneously, to accomplish focusing of both cationic and anionic analytes within the same device [28] – using ICP, this outcome would require integration of both anion and cation permselective nanojunctions into a device. For more information on the mechanistic comparison of fICP and ICP and details on parameters affecting their operationality, the reader is directed to dedicated articles [7,23].

4. Key features relevant to ICP/fICP-based extraction

Broadly, ICP/fICP-based microscale extraction can be categorized into three steps: (i) focusing or preconcentration of analytes, (ii) stabilizing the focused plug, and (iii) extracting the focused plug to another phase (separating it from the original sample). Important aspects of the methods employed to accomplish these steps are discussed in the following three subsections (*4.1 – 4.3*)

4.1. Focusing of analytes

Relative analyte and BGE concentrations and mobilities directly affect electrophoretic and convective responses to the applied electric field, thus defining concentration profiles. Analyte concentration enrichment can occur via focusing or stacking mechanisms. Focusing involves a sign change in the analyte drift velocity affixing the ions along a focal point or region, while, stacking of analyte ions is mediated by a decrease in the magnitude of analyte drift velocity which leads to their accumulation [26]. Focusing can operate under two modes namely, peak and plateau modes. In these two modes, the degree of analyte preconcentration is limited by either electrokinetics or electroneutrality, respectively. Peak mode is exhibited when analytes are present in low or trace abundance relative to BGE ions. Therefore, their contribution to ionic conductance is negligible and the concentration profile of the analyte adopts a peak

shape dictated by the interplay of sequestering forces (convection and electromigration) with diffusional broadening. In contrast, comparable concentrations of analyte and BGE ions give rise to the plateau mode of analyte focusing, wherein the analyte accumulates in a wide band having a limiting concentration dictated by the availability of counter ions of the BGE for charge pairing. Recent works by Ouyang et al. [29] and Papadimitriou et al. [30] have presented detailed expressions to portray dependency of focusing location and separation resolution on analyte mobility, BGE composition, applied potential and device geometry.

For a given analyte, the two competing forces namely, convection (electroosmotic flow (EOF) or pressure-driven flow (PDF)) and electromigration (electrophoresis), balance at a specific axial location along the electric field gradient defined by the IDZ boundary (**Scheme 3**) [23]. Importantly, the electric field strength at which analyte focusing occurs is dependent on the electrophoretic velocity of the analyte and electroosmotic velocity. Electroosmotic velocity (ν_{EOF}) is given by the Helmholtz-Smoluchowski equation:

$$\nu_{EOF} = \frac{\varepsilon\varepsilon_0\zeta}{\eta}E$$

Where ε and ε_0 are relative and vacuum permittivities (F/m), ζ is the zeta potential (V), η is the dynamic viscosity of the liquid (kg/m·s) and E (V/m) is the electric field strength. This equation cannot be applied to systems with nonequilibrium concentration distribution inside and outside of the IDZ (operating within the overlimiting regime) [24].

However, nonequilibrium EOF velocities have been modelled and solved for various systems [31–33]. The electrophoretic velocity of an analyte (ν_{ep}) is proportional to its intrinsic electrophoretic mobility ($\mu_{ep}, m^2/s\ V$) and the applied electric field, E (V/m):

$$\nu_{ep} = \mu_{ep}E$$

μ_{ep} is directly proportional to analyte charge (q), and inversely proportional to the viscosity of the medium (η) and hydrodynamic radius of the analyte (r) as follows:

$$\mu_{ep} = \frac{q}{6\pi\eta r}$$

Electrophoretic mobility is also affected by underlying factors, on which the above-mentioned parameters depend, such as pH (which impacts analyte charge) and temperature gradients (which cause viscosity gradients).

The location of focusing can be controlled with the help of several factors such as by modulating direction or magnitude of the applied electric field or bulk flow rate, by modulating pressure, or by defining the placement and number of ion selective membranes or electrodes. These factors will be discussed in relation to specific advances in upcoming sections of this review.

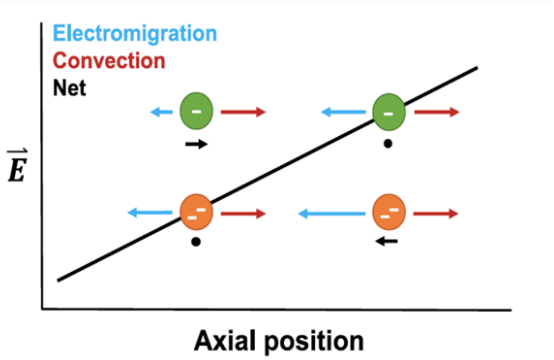

Scheme 3. Electrokinetic focusing of two anionic species having relative higher (orange) and lower (green) electrophoretic mobilities along a gradient in electric field strength. Counter-acting electromigratory and convective forces define the focusing location of each species, where net analyte velocity is zero. Illustration is reprinted with permission from ref [23].

4.2. *Stabilizing the focused analyte plug*

Upon the achievement of a focused plug, it is important to retain the achieved local concentration since dispersion or redistribution of focused analytes will undermine the efficiency of extraction. Existence of secondary EOF or vortex flow which causes analyte dispersion is one of the major concerns of ICP. Fluidic instabilities may be monitored by evaluating current-voltage profiles across the charge selective junction. Depending on the applied voltage, material properties, and device dimensions, the current-voltage profile across an ion permselective membrane can operate in three regimes: ohmic, limiting and overlimiting (**Figure 1**) [24]. Device asymmetry and critical dimensions are known to alter the current rectification factor resulting in currents in excess of limiting currents [34]. For information on current-voltage regimes and mechanisms of vortex formation, the reader is directed to dedicated articles [24,35]. It is the limiting regime wherein the IDZ first develops and the flux of BGE ions becomes limited by their mass transport to the junction. With increasing applied voltage and concurrently induced, dramatic local electric fields, fluidic instabilities or vortices are generated (overlimiting regime). This phenomenon is a result of accelerated ionic velocities (electroosmotic flow) within the IDZ relative to that outside of the IDZ. These instabilities can disrupt the analyte plug and lead to unwanted mixing. Further, under

certain conditions, including high co-ion mobility (the anion for a cation-selective membrane) and increased E, the IDZ continues to grow, propagating away from the

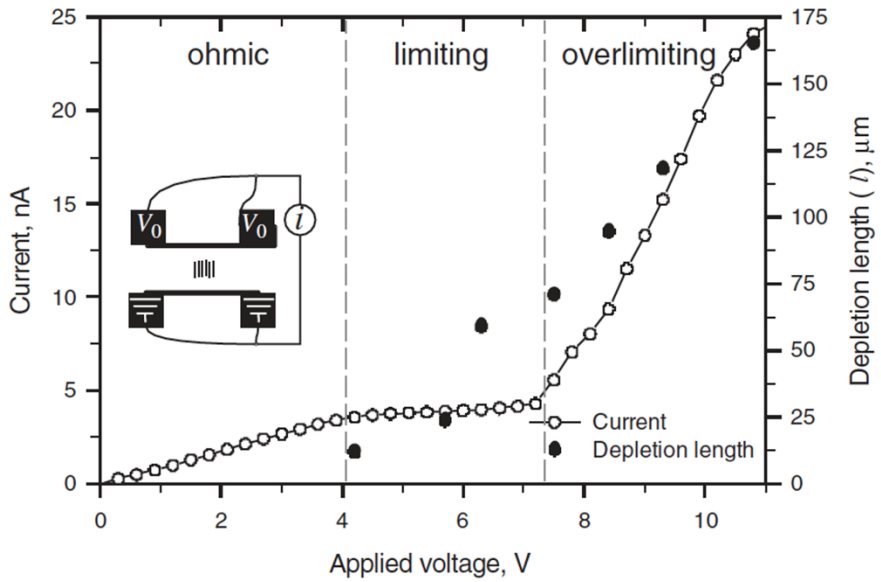

Figure 1. (c) Current voltage plot depicting the typical three regimes – ohmic, limiting and overlimiting current patterns for the ICP phenomenon. Figure is reprinted with permission from ref [24].

junction. In conjunction, fluidic instabilities and IDZ propagation make it challenging to restrict focusing of analytes at a specified location.

Several attempts to minimize fluidic instabilities and secondary EOF have been reported. Mainly, this goal has been achieved by restricting microchannel dimensions [24], using microstructures that segment the channel and promote ion conduction along surfaces [36] such as highly conductive polymer coatings [37], or microstructuring of the micro-/nano- interface to aid in nucleation of small stable vortices [38]. Recently, a 3D electrode comprising metallic microbeads and an additional secondary insulating bead-bed has been utilized to achieve fICP-based stable focusing of anionic analytes – $BODIPY^{2-}$ and dye-linked albumin [39]. The current review highlights approaches adopted in recent works for minimizing instabilities and achieving low dispersion of analyte plugs during extraction.

4.3. *Extraction of the focused analyte plug*

Once the analyte species have been focused into a concentrated plug, the next step is their extraction to another phase or compartment for subsequent analysis. As discussed earlier, the location of a focused analyte plug can be controlled by manipulating factors

such as applied voltage, flow rate, channel dimensions, or electrode placement. Further, such factors can be used to 'move', direct or relocate the focused plug of analytes to a distinct location on the device, in/on to a different phase (e.g., as droplets) or altogether out of the device, thereby achieving their extraction from the original sample.

Droplet and paper-based microfluidic techniques have been widely used to separate and subsequently extract analytes. Droplet-based methods confine analytes to discrete volumes either preceding or following ICP-based focusing and support subsequent manipulation via splitting, merging and sorting. In the case of microfluidic paper-based analytical devices (μPADs), the focused analyte plug can be extracted simply by cutting out specific bands or regions out of the paper-based strip or device. However, there are few ICP-based techniques that capture or extract analytes in/on to a different phase in a manner similar to solid phase or liquid-liquid extractions. Therefore, the use of techniques involving multiphasic ICP-based microextractions is a promising yet underdeveloped area of study.

5. Developments in ICP/fICP-based microscale extraction

Table 1 summarizes the ICP-based extraction techniques for a plethora of analytes ranging from inorganic ions, small charged molecules, bioparticles to larger particles, that are discussed in this review article.

Table 1

Summary of ICP-based extraction techniques for various analytes discussed in this review article.

Type	Analyte	Technique/operational features	Reference
Charged small molecules and inorganic ions	Ca^{2+}, $TrisH^{+}$	In-droplet ICP-based cation exchange and extraction	42
	Fluorescein disodium salt	Droplet generation post ICP-based enrichment	43
	BDP, CB, and AF647	Multitargeted droplet generation post ICP-based enrichment	44
	Li^{+} extraction from a mixture of analytes (K^{+}, Na^{+}, Mg^{2+}, and Cl^{-})	Use of AEMs; simulation study	45
	BDP, CB, and AF647	Free flow-ICP (FF-ICP)	46
	BDP, CB, and AF647	Use of electrophoretic spacers and differential pressure application	30
	Sulforhodamine B and Alexa Fluor 488 dyes	Defined device aspect ratio and differential pressure application	47
	Orange G and Alexa Fluor 488 dyes	3D folding paper-based (μPAD) preconcentrator and extractor	51

Uncharged small molecules	Neutral BODIPY, pyrene	Continuous micellar electrokinetic focusing (CMEKF)	55
Heavy metals	Arsenic, Fe^{2+}, Mn^{2+}, Cu^{2+}, and Pb^{2+}	Integrated ICP and LSV in a radial 8-way channel device	58
Biopolymers	Interleukin-6 (IL-6)	ICP along vertical nanogaps within micropillar arrays	65
	Recombinant green fluorescence protein (rGFP)	Branched flow-through device with narrow upper branch	67
	Excess fluid from blood	Branched flow through device with similar dimensions for both branches	54
	Aptamer sensing	Branched flow device	68
	HIV p24 protein, nucleic acids, human cardiac troponin I protein	Hierarchical nanofluidic molecular enrichment system (HOLMES)	71
	dsDNA	Radial device	59
	MMP enzyme	ICP-based enrichment followed by droplet generation	73
	biotin, (Arg)9, proteins (streptavidin, GFP), and DNA	In-droplet enrichment and separation followed by downstream droplet splitting	74
	Urine proteins and serum amino acids	Cross-type ICP interface in paper-based device	78
	Urine proteins	Integrated ICP and colorimetric detection	79
	Human serum	Sequential ICP in 3D multilayer origami paper-based device	81
Extracellular vesicles	Exosomes	Origami multi-folded μPAD device	85
		Ion selective membrane de-coupled from substrate	86
		Microfluidic gel electrophoresis in combination with ICP	87
Bioparticles	RBCs, *E.coli*	Branched flow through device with narrow upper branch	67
	E.coli	ICP in µPAD incorporated with microwire electrodes	88
Larger particles	Polystyrene particles	Radial device	59
		Orthogonal electric field and flow directions	94
		Bifurcated device. fICP	69
		Trifurcated device, serial fICP	70

5.1 Extraction of charged smaller molecules and inorganic ions

ICP and fICP techniques both involve the application of an electric field and resultant generation of local electric field gradients. It is imperative for charged species to interact with these fields by way of their electrostatic charge, thus facilitating their manipulation. Recently developed methods used to facilitate ICP/fICP-based extraction of charged smaller molecules and inorganic cations and anions are discussed in this section.

5.1.1. Droplet-based extraction

Droplet microfluidics presents advantages such as high-throughput screening, parallel reactions, and low reagent consumption. Additionally, the use of droplets as tiny reaction vessels allows for phase-separated reactions and compartmentalization of droplet components as discrete volumes. Ding et al. summarized recent applications of droplet microfluidics ranging from rare mutation detection, droplet digital polymerase chain reaction (ddPCR), 3D cell culture, to single-cell RNA sequencing, among others [40]. Customized droplet manipulation by merging, sorting, mixing and splitting is now readily achieved and a well-developed area of research. Tenje et al. have summarized internal and whole droplet manipulation using auxiliary methods such as the use of hydrodynamic, acoustic, magnetic, and dielectrophoretic forces, thermal and thermocapillary methods [41]. Once formed, droplets exist as discrete volumes with a defined composition.

In 2020, Kim et al. demonstrated simultaneous cation injection and buffer cation expulsion from nanoliter-scale aqueous droplets [42]. This result is significant as it presents scope for selective ion exchange and extraction in addition to confirming the mechanism of ICP in droplets. The device consisted of a main channel flanked on either side by cation permselective membranes (Nafion®), which extended under the microchannel walls into auxiliary channels. Aqueous droplets composed of 10.0 mM Tris buffer and 10.0 μM Rhod-2 calcium indicator were generated in a continuous oil phase and travelled the length of the main channel. Application of a voltage bias induced in-droplet ICP with influx of Ca^{2+} ions from the 10.0 mM $CaCl_2$-filled anodic auxiliary channel into the droplets and efflux of $TrisH^+$ ions out of the droplets and into the cathodic auxiliary channel. Here, the ICP-induced local electric field gradient facilitated ion movement, while the membranes facilitated ion permselective transport. It must be realized that two distinct extraction processes occur simultaneously. First, extraction of Ca^{2+} cation from the anodic auxiliary channel into the droplet and second, elimination of pre-existing $TrisH^+$ buffer cations out of the droplets and into the cathodic auxiliary channel (**Figure 2**). Droplet composition can be fine-tuned in a way analogous to microtitration; the rate of ion exchange can be controlled through the applied potential, device dimensions and the ionic strength of contents of the auxiliary channels and droplets, which dictate the current. However, it can be challenging to establish the extent of mass transport across the droplets because the electric current is averaged over all droplets that bridge the membranes at any instant. Further, the sample

composition is limited – the BGE conductivity may exceed that allowed by experimental conditions, and pH changes induced by proton transport, in the absence of adequate buffering capacity, can be detrimental to certain classes of analytes. Tailoring experimental conditions to address these challenges in the context of distinct applications is an active area of research.

In the above case, droplet-based ICP focusing and extraction were carried out in pre-formed droplets. Droplets can also be generated and extracted following ICP to

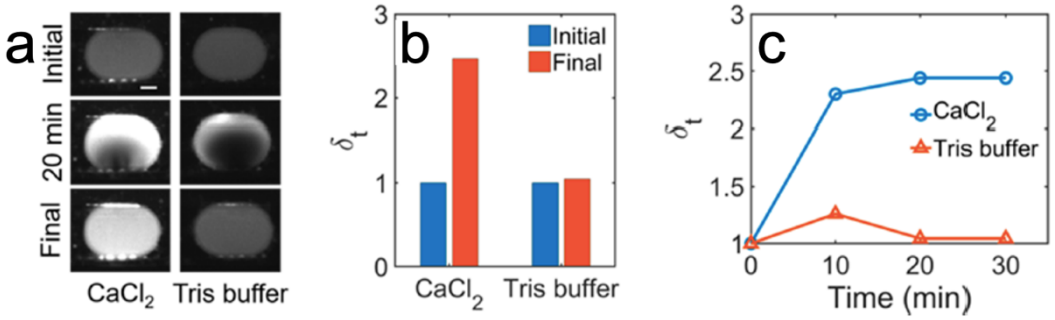

Figure 2. a) Micrograph of droplets confirming Ca^{+2} transport from anodic auxiliary channel into the droplets. For the left set of images, the anodic auxiliary channel was spiked with $CaCl_2$ in Tris buffer (10.0 mM each) while for the set of images on the right, the auxiliary channel contained only the Tris buffer, images were taken before, during, and after application of a voltage bias (5.0 V) across the device; b) Variation in normalized intensity (δ_t) before and after each of these experiments; and (c) Variation of δ_t over the duration of the experiments. Figure is reprinted with permission from ref [42].

"lock in" enrichment. In 2015, Phan et al. integrated a flow-focusing droplet generator downstream of the concentrated output to continuously generate monodisperse droplets of fluorescein disodium salt of programmable size and concentration (100-fold enriched) [43]. ICP induced the focusing and redirection of this fluorescent tracer into a narrow branch of the channel where the concentrated analyte solution was hydrodynamically focused into monodisperse droplets, 25–50 μm in diameter. Importantly, the authors studied the effect of flow rate (10–30 μL h^{-1}) and applied voltage (10–100 V) on the size and concentration of droplets. While focusing prior to droplet generation results in relatively 'analyte-rich' droplets, challenges such as non-uniform droplet composition and dispersion effects within the analyte stream may arise.

ICP has more recently been used to facilitate multitargeted extraction via separation of a mixture of analytes based on their relative electrophoretic mobilities. Papadimitriou et al. integrated multitargeted separation with subsequent droplet generation to obtain concentrated and distinct analyte droplets of three fluorescent tracers, BODIPY disulfonate, Cascade Blue and Alexa Fluor 647 (BDP, CB and

AF647), from a solution [44]. First, ICPF was used to concentrate analytes (1000-fold) based on their electrophoretic mobilities, at a location upstream of the droplet generator. Next, actuation voltage was tuned to shift the distinct analyte-rich bands to the site of droplet generation. Upon the overlap of a specific analyte band in the separation channel with the perpendicularly connected T-junction of the droplet generator (sampling channel), a pressure scheme was applied to extract concentrated analytes as droplets either in droplet-on-demand mode or continuous mode (**Figure 3**).

From the above studies of droplet-based ICP-driven extraction, the following points may be concluded. First, droplet-based extraction may be initiated either prior to or after focusing. In most examples, analyte focusing precedes droplet encapsulation to generate concentrated droplets. However, ICP can also be applied to preformed droplet streams to achieve focused regions or zones within the droplets. Extraction in this case can be achieved in two ways: (i) Analytes can be either injected into or expelled from droplets. This operation is similar to microtitration due to the controlled rate of exchange. (ii) Sample droplets can be focused and then split into corresponding analyte-rich and analyte-deficient daughter droplets using a downstream splitting junction. Second, factors such as applied voltage, flow rate, and pressure can be used to define or shift the focusing location, thereby exerting spatial selection of the species to be extracted. Third, the extracted analyte-rich droplets can be subjected to subsequent downstream analysis or manipulation (merging, sorting, splitting). Droplet-based ICP-mediated extraction presents phase-separated, volume-specific, high-throughput and quantitative extraction of low-abundance analytes. However, the main challenge of obtaining uniform droplet composition and quantifying in-droplet analyte concentration persists.

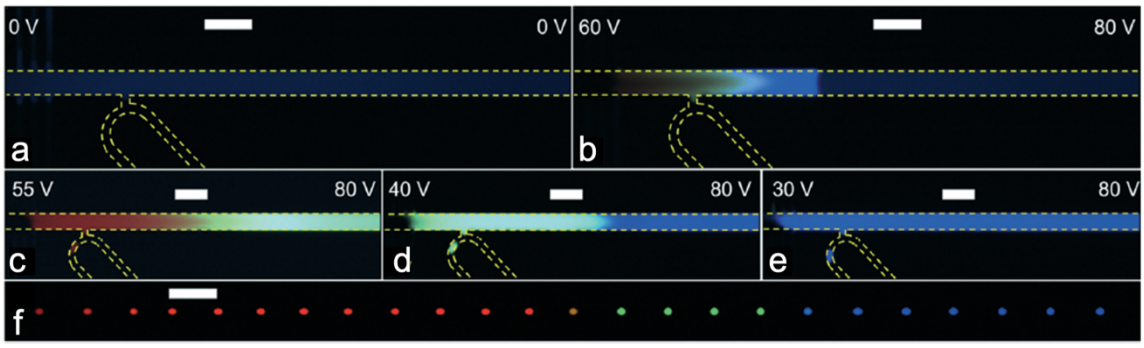

Figure 3. Extraction of separated analytes as droplets. a) Initial system with no application of voltage or pressure; b) Initiation of ICP focusing of analytes at t ~1s at a voltage bias of 60 V; c) Tuning of actuation voltages post ICPF to move AF647 analyte band and produce a single droplet on demand; d) Shifting of focused BDP plug and subsequent droplet generation; e) Shifting of CB focused plug and extraction of single droplet; f) Separate experiment for continuous droplet generation over a duration of 5 min (scale bars, 100 μm). Figure is reprinted with permission from ref [44].

5.1.2. Use of anion exchange membranes (AEMs)

The use of cation selective membranes is more widespread in ICP techniques, mainly due to the prevalence of materials with negatively charged surface groups and well-characterized off-the-shelf reagents such as Nafion®. However, anion exchange membranes (AEMs) (e.g., Sustainion®) can also be used to facilitate selective ion transport. Gong et al. developed a two-dimensional numerical model for selective Li^+ extraction from a mixture containing Li^+, K^+, Na^+, Mg^{2+} and Cl^- [45]. In this model, a transmembrane voltage ($100V_T$, where $V_T \equiv$ thermal voltage of 25.8 mV) across the AEM resulted in the transport of Cl^- ions through the membrane and generation of an IDZ and IEZ in the cathodic and anodic compartments, respectively. Cations in the cathodic compartment are repelled away from the AEM junction and focus at distinct locations upstream.

AEM-mediated ICP-based extractions can be employed to either selectively extract anions as in the case where Cl^- ions accumulate in the IEZ at the cathodic compartment or to focus and subsequently extract cations from the anodic compartment. In the above example, the authors employed external pressure to control fluid flow velocities for extraction of cations into the downstream reservoir. In practice, any of the alternate methods of extraction developed for use with cation exchange membranes (CEMs) could be leveraged for AEM-mediated extraction. The development of a wider range of AEMs compatible with ICP-based systems would be a fundamental step towards exploring more applications. Features including high ionic conductivity, biocompatibility, and minimal swelling in aqueous environments are desirable.

5.1.3. Free flow ICP

Recently, Papadimitriou et al. developed a new technique called free flow ICP (FF-ICP) to improve resolution during continuous, high-throughput focusing and extraction of anionic analytes (BDP, CB and AF647) [46]. The highlight of this technique is that the electric field is predominately perpendicular to the direction of flow (EOF/PDF), enabling a longer duration of interaction of the analytes with the electric field. To establish this orthogonality, the authors incorporated an intricate set of channel arrays connecting left and right reservoirs to the main separation channel. These arrays

provided a high resistance path for current passage, thus minimizing transverse current flow. Further, the use of a Nafion® microbridge array minimized IDZ instabilities (**Figure 4**). This approach yielded an increased number of theoretical plates. Moreover, simultaneous co-focusing of two analytes in peak mode with an electrophoretic 'spacer' of intermediate mobility in plateau mode was used to achieve improved separation resolution. The spacer (green dye, **Figure 4d**) focused between two analytes thereby spacing them apart by creating there a local plateau in the electric field.

From this work, it can be noted that device architecture plays a prominent role in ensuring orthogonal orientation of flow and electric fields, and in minimizing fluidic instabilities at higher voltages. Further, this orthogonality increases the length (and therefore, the duration) over which the separands interact with the field gradient, thereby increasing resolution. This work also demonstrates the use of electrophoretic spacers in the context of continuous separations. Development of spacers having a wide range of distinct electrophoretic mobilities is critical to the advancement of this approach.

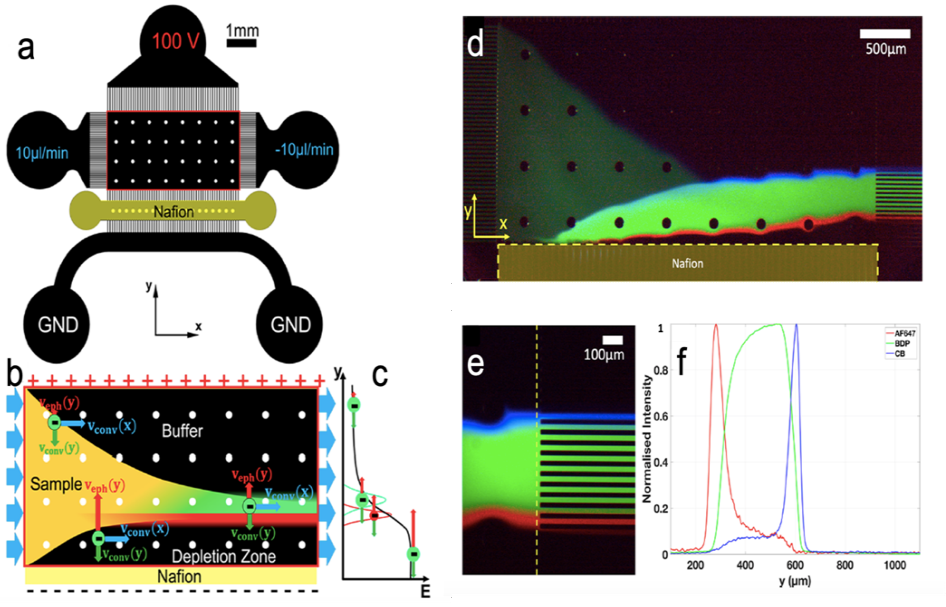

Figure 4. a) Schematic of the FF-ICP device; b) Operating principle of FF-ICP employing orthogonal directions of PDF ($v_{conv(x)}$) and applied E-field; c) Plot of focusing locations of analytes in y-direction; d) Fluorescence micrographs showing focused streams of CB, BDP and AF647; e) Zoomed-in image of the extracted streams in (d); and f) Normalized fluorescence intensity profiles of CB, BDP and AF647 vertically along the yellow line of image (e), BDP (focused in plateau mode) acts as an electrophoretic spacer between CB and AF647 which focus in peak mode. Figures are reprinted with permission from ref [46].

5.1.4. Pressure modulation to deplete abundant species

In a report published by Papadimitriou et al. in 2019, continuous extraction of anionic analytes (BDP, CB and AF647) with high concentration factors (300-fold) and resolutions was achieved by combining two key aspects – differential pressure

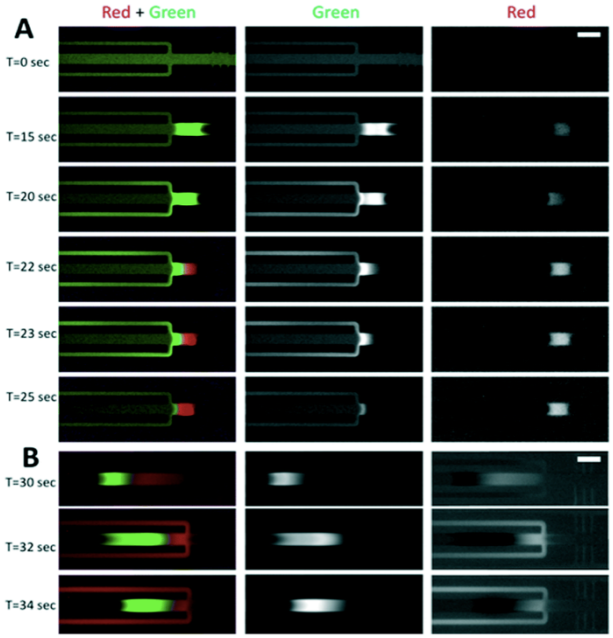

Figure 5. Composite green and red fluorescence images showing the separation and extraction of BDP (green) and AF647 (red) from their mixture (in 0.1× PBS). Distinct set of actuation voltages are applied in the two separate experiments A) V = 60 V and V = 30 V and B) V = 60 V and V = 55 V, to extract BDP and AF647, respectively (scale bars, 100 μm). Figure is reprinted with permission from ref [30].

application and use of electrophoretic spacers [30]. A mixture of analytes subjected to ICP underwent enrichment and separation into discrete bands, which were then extracted by controlling the voltage and applying negative pressure along the two extraction channels (**Figure 5**). The authors describe the application of an initial actuation voltage, followed by a 'wait' time to ensure the required concentration factor and then adjustments in the voltage bias to steer the focused plug to the extraction channel, where a negative pressure facilitated extraction. Device architecture plays an important role with the perpendicular placement of separation and extraction channels to effect pressure-driven extraction of focused analyte plugs.

This approach builds on an earlier study by Choi et al. in 2015, where an interplay of device architecture and differential pressure application was used for selective and high resolution extraction (demonstrated with Sulforhodamine B and Alexa Fluor 488 dyes) [47]. Preconcentration of analytes (100-fold) within separate microchambers of defined aspect ratio was facilitated by ICP. Further, the analytes were extracted from these microchambers using pneumatic microvalves. While the use

of pneumatic valves complicates fabrication and operation, this aspect has been addressed in alternative scaffolds such as μPADs by incorporating passive flow regulation strategies [48]. In the above advancement by Choi et al., the use of nanochannels is a noteworthy strategy to allow narrow and well-resolved plugs to be maintained during extraction.

5.1.5. Paper-based extraction

μPADs have revolutionized analytical techniques by presenting advantages such as low cost, portability, ease of use and fabrication, and disposability, which are well-suited to point-of-need implementation. Moreover, the capillarity offered by paper-based materials overrules the need for additional pumps or pressure modulation for fluid to be flowed. Several recent advances of μPADs in clinical and environmental applications have been summarized by Ozer et al [49]. Challenges in the use of μPADs include reduced fluid control, evaporation, poor limits of detection, considerations for stability and shelf-life of devices when incorporating assay mixtures or biological reagents, and material restrictions in properties such as porosity and wettability [49,50]. For ICP/fICP-mediated μPAD-based extractions, additional challenges may be incurred. First, Joule heating induced by the applied electric field should be withstood by the μPAD. Second, material properties such as variable porosity as well as analyte-paper interactions (adsorption) may intervene with electrophoretic and electroconvective forces. Finally, the volume into which the analyte is focused is relatively large (on the order of 100 nL–1 μL), while the volume of fluid swept by ICP (tens to hundreds of microliters) is limited by the capacity of the sample and waste pads, which if exceeded, leads to overflow. Under these constraints, 10- to 1000-fold enrichment is expected.

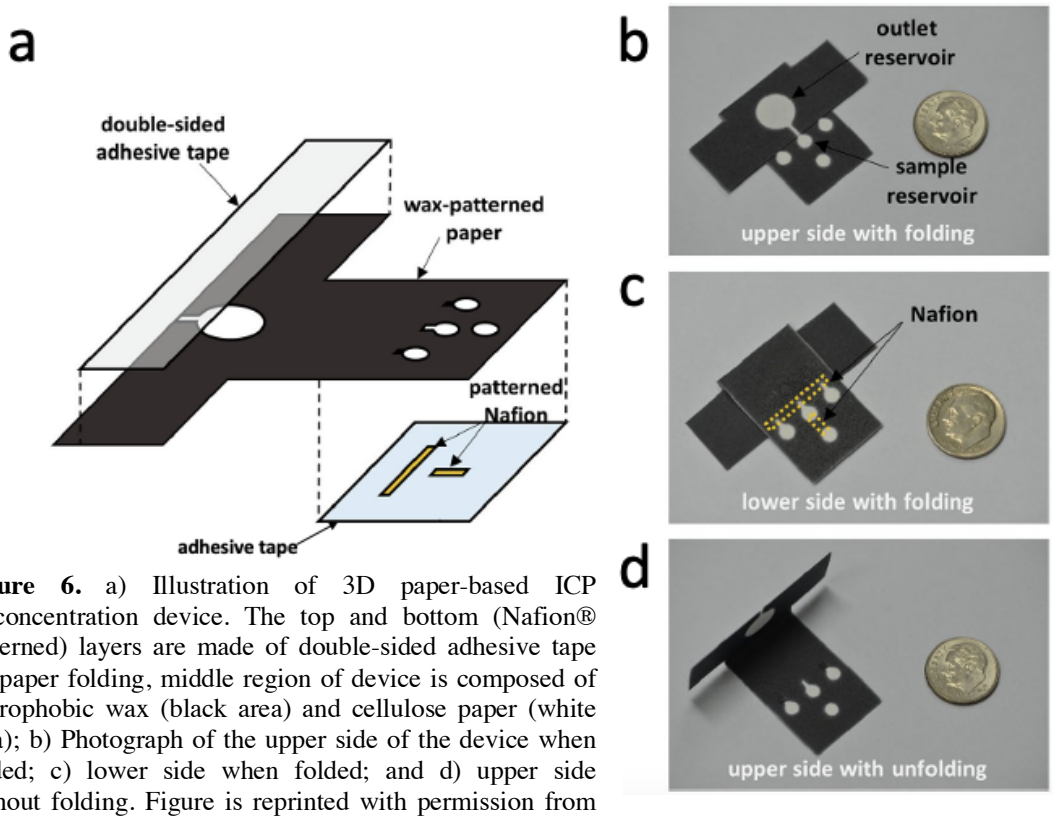

Figure 6. a) Illustration of 3D paper-based ICP preconcentration device. The top and bottom (Nafion® patterned) layers are made of double-sided adhesive tape for paper folding, middle region of device is composed of hydrophobic wax (black area) and cellulose paper (white area); b) Photograph of the upper side of the device when folded; c) lower side when folded; and d) upper side without folding. Figure is reprinted with permission from ref [51].

Lee et al. developed a wax-coated folding paper-based preconcentrator and extractor and demonstrated its function within negatively charged Orange G and Alexa Fluor 488 dyes [51]. ICP was used to generate a 300-fold concentrated analyte plug from a minute sample volume of 10 μL within 10 min. The concentrated plug was maintained with minimal dispersion even during actuation of a folding 3D pop-up outlet which disconnected fluidic contact (**Figure 6**). The sample reservoir with concentrated analyte plug was simply cut out for further analysis.

While ICP-mediated μPAD-based extraction provides facile focused-analyte collection, important questions remain. First, the implementation of μPADs at the point of need raises the issue of how best to integrate preconcentration with in situ analysis. Second, it must be determined whether μPADs can be utilised for the extraction of analytes from native media. Recent advances utilising ICP for paper-based analyte preconcentration from native media will be discussed in *Section 5.4.3.* of the current review.

Advancements in the fabrication of μPADs, such as the development of hybrid 3D-printed μPADs, promise to tackle issues related to material properties, fluid control and operationality [52]. An interesting area of study would be to harness the analyte-paper interactions as a means for the extraction of analytes such as by the use of chemically modified paper or by the impregnation of the paper with sorbent beads.

5.2. *Extraction of uncharged small molecules*

Electrokinetic manipulation of charged analytes over uncharged species is more common, simply because their intrinsic charge experiences electrostatic force. However, extraction of uncharged analytes under an applied electric field, as in the case of ICP/fICP techniques, can be accomplished by exploiting their interactions with other chemicals or additives. In micellar capillary electrophoresis or micellar electrokinetic chromatography (MEKC), analytes are separated based on their interactions (electrostatic, hydrophobic and steric, among others) with a charged micellar pseudostationary phase. The neutral species thus acquire 'apparent charges' through partitioning into the micelles [53]. The extraction of neutral analytes can therefore be achieved based on the extent of analyte-micelle interaction and acquired charge.

Preliminary results from ICP focusing of a neutral dye (BODIPY FL) suggested the possibility of extracting it from blood plasma (while the same electrokinetics were not observed in an aqueous buffer) [54]. In this case, extraction was attributed to the interaction of charged components of the blood plasma with the dye. Taking inspiration from this observation and applying analogy from MEKC, Berzina and Anand leveraged ICP to focus micelle-encapsulated neutral analytes, as a means for their continuous extraction, coining this technique continuous micellar electrokinetic focusing (CMEKF) [55]. Local enrichment of surfactants along the IDZ boundary was achieved under the application of a voltage bias across a membrane positioned just downstream of a branching junction in a microchannel (**Figure 7**). Subsequently, local guest-host pairs were formed between resulting micelles and neutral analytes (BODIPY FL, pyrene). By virtue of their interaction with these charged micelles, neutral molecules are excluded from the IDZ and streamlined into a separate outlet (upper branch, **Figure 7**) of the microchannel, thus facilitating their extraction. An important point to note is

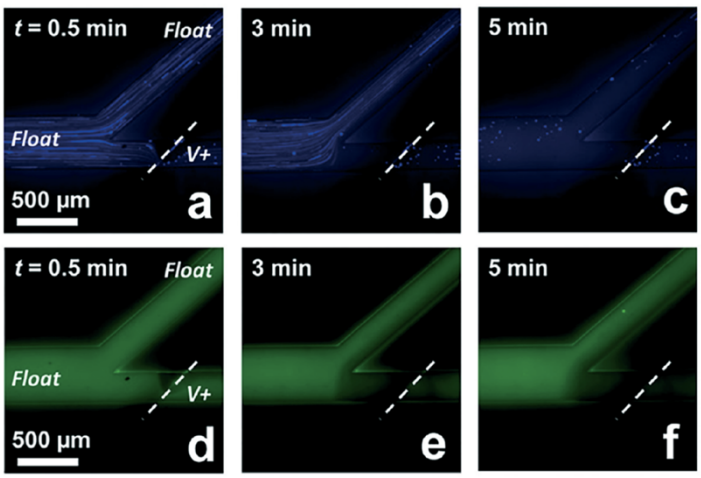

Figure 7. Fluorescence micrographs showing the continuous focusing and solvation of the neutral species: (a-c) pyrene (blue); and (d–f) BODIPY FL (green) in the presence of sodium cholate surfactant in phosphate buffer (pH 7.4) at a flow rate of 60 nL min^{-1} and V^{+} = 60.0 V. The white dashed line represents the location of the patterned Nafion® membrane. Figure is reprinted with permission from ref [55].

577 the deviation from MEKC, in which ionic micelles form at surfactant concentrations
578 only above the critical micelle concentration (CMC) in the bulk solution. However,
579 CMEKF enabled the focusing of neutral analytes at bulk surfactant concentrations an
580 order of magnitude below the CMC through local enrichment and assembly of
581 surfactants into micelles. Selective extraction from a mixture containing several neutral
582 compounds is anticipated given that the target separand has a distinctly high micelle-
583 water partition coefficient, K_{mw}, which lends it a high effective electrophoretic
584 mobility.

585 It may be concluded that, neutral analytes can be electrokinetically extracted only
586 after inducing a pseudocharge on the analytes by way of interactions with charged
587 species such as ionic micelles. A major limitation is that extraction efficiency in such
588 cases calls for maximum interaction (K_{mw}) between the micellar and analyte species
589 and the number of available surfactant sites at the interface region, which depends on
590 the concentration and solubilization capacity of the micelles. Thus, hydrodynamic
591 focusing of micelle-encapsulated analytes along with the continuous and stabilized
592 enrichment of surfactant molecules near the IDZ, must be optimized to effect maximum
593 extraction efficiency. Equally important is the chemical nature, charge, electrophoretic
594 mobility and concentration of the charged additives (surfactants).
595
596 *5.3. Extraction of heavy metal ions*
597 Heavy metal ions are known to have detrimental effects on health and the environment,
598 even when present in trace amounts. Thus, they qualify as low abundance analytes that
599 require qualitative as well as quantitative detection and extraction. Several microfluidic
600 techniques for electrochemical detection of heavy metal ions have been developed. So
601 far, cyclic voltammetry, anodic stripping voltammetry (ASV), square-wave ASV, and
602 colorimetric detection methods have been used [56,57]. In a first report of ICP-
603 mediated heavy metal ion preconcentration and detection, Subramanian et al. integrated
604 ICP with linear sweep voltammetry (LSV) for on-chip quantitative detection of arsenite
605 and other heavy metal ions (Fe^{2+}, Mn^{2+}, Cu^{2+} and Pb^{2+}) in the presence of H_2SO_4
606 solution [58]. Here, the authors employed a radial 8-way channel device with a central
607 well, which housed working (WE), counter (CE) and reference electrodes (RE). A
608 circularly patterned Nafion® membrane intersected the channels. During operation, a
609 driving voltage applied between the central well (Pt wire anode) and the channel outlets
610 led to the enrichment of both anions and cations in the central well. The accumulation

of cations near the anode was attributed to a need for electroneutrality – cations charge paired with anions accumulating there. However, this proposed mechanism does not account for the relatively higher concentration of protons within the acidic medium and those generated faradaically at the Pt anode to redistribute to maintain electroneutrality.

An alternative method for the enrichment of cationic species would be to use an AEM and reversed polarity to drive focusing, which would be more effective in restricting cation mass transport away from the junction towards the central well. In such a configuration, the metal ions would be deposited onto the central cathodic driving electrode, which could then double as the WE. A similar radial buffer channel-less device with a CEM had been developed for the extraction of negatively charged analytes including polystyrene particles, dyes and dsDNA [59]. In this device, enriched analytes were extracted by pipetting solution from the central well following enrichment.

5.4. Extraction of biopolymers: proteins and nucleic acids

In this section, we will discuss ICP/fICP-based extraction of biopolymers such as peptides, proteins, and nucleic acids. These extractions are carried out in microfluidic devices in preparation for bioanalysis. Chiu et al. recently discussed opportunities for microfluidic technologies, highlighting applications in genomics, single-molecule and single-cell analysis, cancer cell studies, and mimicking physiologic systems [60]. In many such systems, preparation of the sample, including biomolecule extraction is carried out prior to its introduction onto the chip, thereby increasing manual intervention by the operator. These off-chip processes leverage solid phase or liquid-liquid extraction techniques or affinity chromatography. For example, Vicente et al. have discussed the literature on liquid-liquid extractions using two-phase systems for separation and purification of proteins and nucleic acids [61]. Electric-field driven extractions are readily miniaturized and automated, and therefore, they are well-suited for integration into microfluidic platforms for bioanalysis.

Several factors need to be considered for the electrokinetic manipulation of biopolymers. During their subsequent analysis, specificity is accomplished via biorecognition events (e.g., protein-protein, aptamer-protein, DNA-DNA interactions) that are susceptible to disruption in the slightest presence of contaminants, pH change or temperature change. Therefore, it is important to maintain a viable chemical and physical environment for proper functioning of bioanalytes, during and post their

manipulation. Important attributes of this environment discussed briefly in the following paragraphs include local pH gradients within the device, the ionic strength and mobility of the BGE, and the propensity of device materials for nonspecific binding.

A particular challenge for methods that leverage ICP and fICP phenomena is that they induce pH changes affecting the local chemistry near permselective membranes or electrode interfaces. Changes in pH occur because of ion-selective mass transport or faradaic reactions resulting in the variation in local concentrations of H^+ or OH^- ions. For this reason, the buffering capacity of the BGE needs to be high.

However, the ionic strength and conductivity of the BGE, as well as the mobility of the BGE ions, play a central role in determining the degree of analyte enrichment, the extent of Joule heating, and the upstream propagation of the IDZ from the junction. For example, a highly mobile co-ion favors both tight focusing (in peak mode) and IDZ propagation. Further, as the local ionic strength contributed by the analyte approaches that of the BGE (within about 10-fold), its enrichment reaches a limit dictated by electroneutrality. Conversely, a more concentrated BGE facilitates Joule heating as well as high current that shift pH and can damage the membrane or electrode. Therefore, optimal performance is anticipated in a BGE comprised solely of buffer ions (not salts), for which the co-ion has a high mobility, present at a moderate concentration (at least 10-fold the targeted post-enrichment concentration of the analyte). For an anionic analyte, cationic buffers such as Tris/$TrisH^+$ with high mobility anions (halides, NO_3^-, ClO_4^-, SO_4^{2-}) are widely utilized. In this context, a low cation mobility is a preferable route to reduce Joule heating, current density, and fluidic instability.

Non-specific binding along channel walls and membranes is another important challenge which can be minimized using polymeric coatings to alter zeta potentials and increase hydrophilicity. For example, block copolymers of ethylene oxide and propylene oxide are commonly employed [62,63].

The following three subsections (*5.4.1 to 5.4.3*) examine recent advancements in biopolymer extraction by ICP in single and multiphase systems as well as in μPADs.

5.4.1. Biomolecule extraction in single-phase systems

In this subsection, we discuss modifications to the device construction and operation that address four challenges for biomolecule extraction facilitated by ICP: 1) the need for a robust and reproducible junction, 2) biofouling of the electrodes or membranes, 3) low enrichment factors due to limitation in the volume swept, and 4) the need for user-friendly sample recovery following enrichment.

In 2018, Hong et al. reported the first demonstration of preconcentration (100-fold in 10 min) and electrochemical detection of methylated DNA on a single chip by integrating an ICP-based preconcentration unit and an electrochemical sensing unit, which leveraged methyl domain binding protein-decorated silica nanoparticle labels to block the approach of a negatively charged redox species to the electrode surface, thereby amplifying the signal [64]. Moreover, low limits of detection were achieved for the electrochemical detection of the methylation of glutathione-S transferase-P1 (GSTP1, LOD 7.9 pM) and extracellular matrix protein 1 (EFEMP1, LOD 11.8 pM) in human urine sample spiked with these genes.

Work by Lu and Maharbiz, addressed the need for a robust and reproducible junction in their device designed for preconcentration and detection of a low-abundance protein (IL-6) [65]. Here, vertical nanogaps within silicon micropillar arrays were used to render ICP. In this study the use of vertical nanogaps parallels a permselective membrane by facilitating selective ion transport. These nanogaps were fabricated between Si pillars via oxide layer growth, which gradually narrowed the gaps in a controlled manner. The authors then extended the technique for bead-based immunoassays by the incorporation of functionalized beads within the micropillar assembly. The incorporation of a solid substrate is a strategic step towards phase-separated extractions.

In an interesting study by Sabbagh et al., pressurized deformation valves were used to create nanochannels for ICP-driven biopolymer enrichment and extraction onto affinity beads [66]. The dynamic tunability of the ion-permselective junction in this device presents multiple advantages such as parallelized preconcentration, control over sensing location, and opportunity for multiplexed detection.

Branched microchannels can leverage ICP to continuously preconcentrate proteins and cells, such as RBCs and *E.coli*, for subsequent analysis [67] and to regenerate an aptamer-based sensor by procuring target-free solution from the biofluid comprising the sample [68]. Such devices can undergo biofouling if these species contact electrodes or membranes, leading to sample degradation and loss of device

function over time. Berzina et al. reported a method to perform ICP-based continuous separations in blood plasma with minimal biofouling [54]. In this separation, plasma proteins were redirected into one branch via ICPF while excess fluid, along with some neutral metabolites, was extracted from the other 'desalted' branch, which was occluded by the IDZ. The device had two key features. First, the Nafion® membrane was located more than 100 μm past the branch point and into the desalted branch, and therefore, it was protected from interaction with cells and anionic species by the IDZ (**Figure 8b**). Second, the device was configured to ensure no contact between blood plasma and driving electrodes, which were located solely in the outlet to the desalted stream and in the auxiliary channel reservoirs. The potential at the sample inlet and remaining outlet were left floating.

Based on these reports, it may be concluded that branched flow-through devices

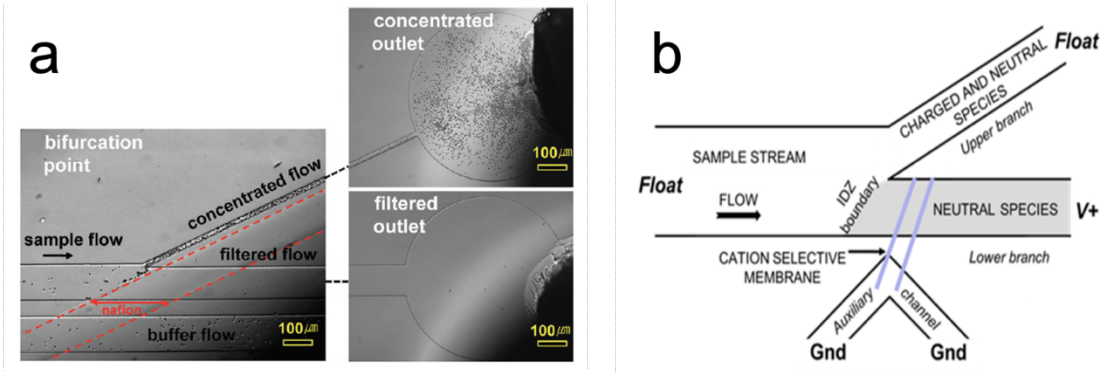

Figure 8. a) Brightfield micrograph of the region of ICP operation (left) of the continuous-flow concentrator device and corresponding outlets (right) for the collection of concentrated and filtered flows. Figure is reprinted with permission from ref [62]; b) Branched flow device with equivalent aspect ratios of the two branched channels, floating potential at the inlet and "salted" outlet, and with the Nafion® membrane patterned farther into the IDZ. Figure is reprinted with permission from ref [54].

offer two-way extraction of manipulated analyte streams, and the location of the permselective membrane/s and electrodes is critical to prevent biofouling. Bifurcated and trifurcated devices have also been used for fICP-mediated extraction of microbeads [69] and microplastics [70], which will be discussed in *Section 5.7.3.* of the current review.

In 2019, Ouyang and Han developed an ICP-based universal biomolecule enrichment system named HOLMES (Hierarchical nanofluidic molecular enrichment system). This approach addresses one of the primary limitations of ICP-based extraction methods – mass transport of the analyte(s) to the IDZ boundary. HOLMES comprises massively parallel and hierarchically cascaded nanofluidic concentrators,

which facilitate billion-fold enrichment of NAs and proteins within 30 min [71]. The key feature of the design is that the critical dimensions were maintained sufficiently low (tens to hundreds of microns) to suppress fluidic instability (vortices) while sweeping a much larger sample volume on the order of 10 mL. This strategy was implemented through cascading preconcentration steps in successively narrower segments across the four stages of the device; the first stage comprised 38,400 parallel preconcentrators (each defined by a microscale channel) and the last, only one. The enriched analyte plugs were swept out (and re-concentrated) from one stage to the next by closing the side outlets of the preceding stage and opening those of the succeeding stage (at modulated voltages) until the analyte plug was finally re-concentrated to a single microchannel at the last stage.

Finally, the need for recovery of the focused analyte has driven the development of radial preconcentrators, in which the analyte is extracted from a central port. In 2011, Sinton and coworkers introduced a finned radial chamber geometry, which achieved a high efficiency and speed of preconcentration in addition to minimized fluidic instabilities and a high volume capacity for sample loading [72]. In this device, the focused plug was injected electrokinetically via a centrally positioned vertical channel into an overlying analysis layer comprising a single microchannel. Building on this concept, a buffer channel-less radial preconcentrator and extractor for dsDNA was developed in 2019 by Kim and coworkers [59]. Herein, application of a voltage bias across a circularly patterned membrane resulted in the upstream propagation of focused analytes away from the developed IDZ and towards a central reservoir housing a pipette tip (**Figure 9**). Concentrated analytes were extracted by simply pulling the pipette tip out of the central well. In the same work, the authors leveraged faradaic reactions for fICP-based preconcentration and extraction of either positively or negatively charged species (demonstrated with rhodamine 6G and sulforhodamine B dyes). In this case, instead of a circular membrane, an electrode was incorporated by printing silver ink using an inkjet printer.

One of the major challenges noted in these techniques was the generation of bubbles at the central electrode tip leading to possible interruption of the electric field. Additionally, lower-than-expected preconcentration levels were observed as a result of diffusion in the central well (prior to voltage application) or advection while pulling out

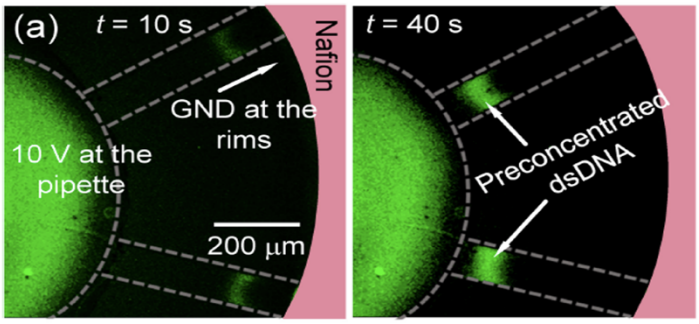

Figure 9. Micrographs showing preconcentration of double-stranded DNA in two of the microchannels of a radial device. The anode is connected to the central well while the cathode is a ring electrode present near the rim of the radial device. ICP drives the concentration and focusing of analytes toward the central well with time. Figure is reprinted with permission from ref [59].

the pipette tip. Despite these limitations, the radial microchannel configuration has a major advantage in that it allows for user-friendly sample recovery. Further, this configuration when combined with techniques such as LSV at a central electrode (*Section 5.3.*) can provide in situ quantification of analyte concentration. In a similar vein, there is scope for the incorporation of a second phase in this reservoir to facilitate liquid-liquid or solid phase extraction.

5.4.2. Biopolymer extraction in multiphase systems

As discussed in *Section 5.1.1.*, ICPF can be facilitated before [43] or after [42] sample encapsulation in droplets and is useful for pre-enrichment for biomolecular assays and extraction of chemical species into and out of droplets. In a study by Chen et al., enrichment prior to droplet formation was leveraged to enhance an enzymatic assay [73]. Herein, a diluted enzyme solution was focused using ICP. The external voltage bias was subsequently removed, and pressure driven flow was employed to drive the plug of enzyme towards a mixing zone where a solution of a suitable fluorogenic substrate was introduced through side channels. The resulting solution was encapsulated as monodisperse droplets with varying enhanced enzyme and constant substrate concentrations. The droplets thus acted as tiny reaction vessels facilitating enzymatic assay. While ICPF enabled enzyme enrichment, the dispersion of enriched plug upon switching off the voltage and during its transport needs to be remedied.

In an interesting study by Saucedo-Espinosa and Dittrich, in-droplet separation and enrichment of peptides, proteins, and nucleic acids was achieved [74]. Here, a water-in-oil droplet stream was contacted with two parallel, carbon-doped PDMS conductive membranes, bridging liquid electrodes (electrolyte-filled auxiliary channels) and a main (droplet-containing) channel (**Figure 10**). Upon application of a driving voltage to the liquid electrodes, an anionic tracer, fluorescein is observed to accumulate near the anodic membrane. Importantly, the incorporation of a branch point downstream of the membranes allows separation of fluorescein rich and depleted regions as daughter droplets. Besides fluorescein, the authors quantified the enrichment

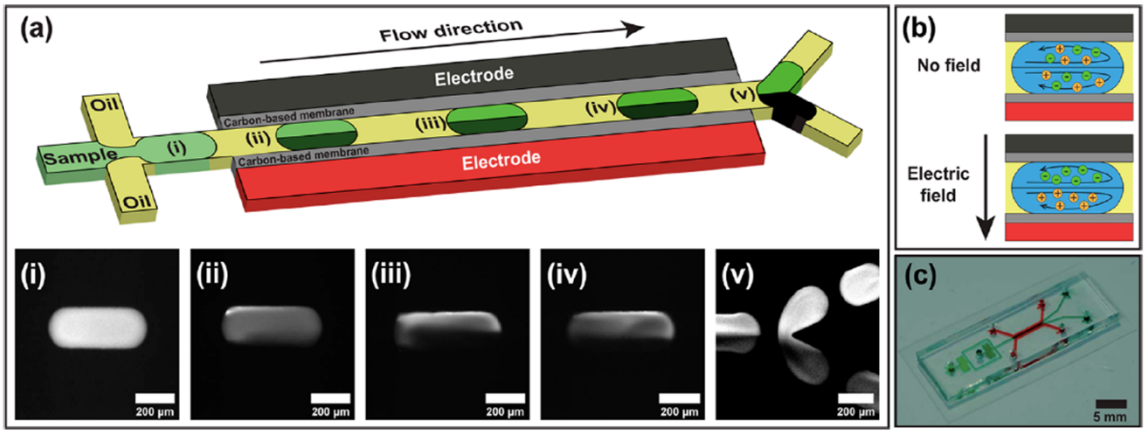

Figure 10. a) Schematic of the integrated microfluidic device used for droplet generation, enrichment, and separation. Droplets of the sample are hydrodynamically generated and enter the region of the device sandwiched between two liquid electrodes which are connected to the flow channel by carbon-based PDMS membranes; i-v) show the sequential process of in-droplet enrichment, separation and downstream splitting as the droplets traverse the flow channel; b) Schematic showing charge-dependent analyte recirculation upon voltage application; and c) Photograph of the microfluidic device with the flow channel dyed green and liquid-electrode channels dyed red. Figure is reprinted with permission from ref [74].

of small molecules (biotin, (Arg)9), proteins (streptavidin, GFP), and DNA, which ranged from 1.5 to 2.0 fold. The authors attribute this enrichment to linear electrophoretic processes driven by the capacitance of the conductive PDMS. The similarity of this result to the ICP-based in-droplet concentration enrichment reported by Kim et al. [42], provides opportunities for the development of extraction techniques based on in-droplet enrichment followed by splitting. A key point is that, in the ICP-based mechanism, the cathodic hemisphere of the droplet is depleted of both signs of charge carriers and exhibits vortex flow, whereas linear electrophoretic processes will lead to accumulation of cations near the cathodic membrane and no vortices, though charge-dependent recirculation effects exist.

Electrokinetic methods for enrichment and separation of biomolecules in the context of droplet microfluidics hold promise for enhanced bioassays. This burgeoning

field would benefit from further study into communication between the membranes or electrodes and the droplets, the role of continuous phase composition, droplet-confined fluid dynamics, and gradients in droplet interfacial properties. Moving forward, extraction into droplets is an intriguing possibility as it could be leveraged to reveal spatial distribution of analytes (e.g., in tissues).

5.4.3. Biopolymer extraction in paper-based devices

As discussed in *Section 5.1.5.*, μPADs present an advantage for extraction in that the analyte can be recovered by folding away or cutting out the paper segment containing the enriched plug. There are several works that have utilized ICP in μPADs to achieve concentration enrichment of biopolymers such as nucleic acids and proteins up to several hundred fold [75–77]. Here, challenges specific to ICP-mediated biomolecule extraction in the context of μPADs are discussed.

First, non-specific interactions of biological samples must be considered when using cellulosic materials. Due to its greater hydrophilicity and negatively charged surface, nitrocellulose exhibits lower non-specific binding of many biomolecules, and anions in particular. In the context of electrokinetics, it is important to note that the large negative zeta potential of this material (−16 to −34 mV) augments electroosmotic flow. Coatings containing surfactants and blocking agents, such as BSA, can similarly diminish non-specific adsorption (NSA) and modify surface charge. Some pretreatments commonly employed for μPADs (e.g., Stabilguard®) have high ionic strength, which exacerbates Joule heating, and in this aspect, non-ionic surfactants are anticipated to perform best for ICP in μPADs.

Second, pH and temperature gradients associated with ICP, must be closely monitored due to the often large contact area between air and/or membranes and paper, and high current densities. Particularly problematic, is that cation permselective membranes are highly acidic and can lower the pH of the paper strip by several units if not soaked in aqueous solution usually overnight. Such pH changes alter the charge state of biomolecules, which in turn impacts their electrophoretic mobility, solubility, and stability. Current at membranes and electrodes can also introduce H^+ and OH^- into the paper medium. These currents also drive Joule heating, which together with air exposure put the μPADs at risk for drying out. For this reason, electrokinetics are often carried out in paper strips that are laminated or dipped into fluid-filled reservoirs.

Finally, underlying effects associated with material properties including non-uniform porosity and wettability could also lower the quality of focusing and separation resolution. We anticipate that these limitations can be overcome by the development and design of more homogeneous and compatible materials or coatings for μPADs.

The preconcentration of analytes from native/complex media, is being increasingly explored, opening new avenues for their further extraction. However, high ionic strength and abundance of biomolecules in native media such as blood, sweat, urine, and saliva, deter ICP. Therefore, strategies to overcome the limitations of BGE concentration and interference to ICP is necessitated. In 2019, Chen et al. employed a cross-type ICP interface comprising intersected paper strips sandwiching either a CEM or AEM for the direct processing and preconcentration of urine proteins and serum amino acids [78]. The use of a cross-type interface instead of the conventional parallel interface rendered a more robust electrical contact and enhanced tolerance to BGE ionic strength. Gao and coworkers used ICP to achieve 60-fold stacking of total protein from clinical urine samples that enabled their colorimetric detection [79]. Han et al. employed a Nafion-reservoir-Nafion device configuration to preconcentrate analytes in blood-based biofluids which have high ionic strengths [80]. An innovative study by Lee et al., leveraged sequential ICP in a 3D multilayer origami paper-based device to achieve 13-fold preconcentration of human serum [81]. Their utilization of sequential ICP overcomes the limitation of high ionic strength of the sample by circumventing the requirement for high voltage application. The use of 3D folding successive layers is convenient for separating the preconcentrated analyte after the enrichment step.

5.5. Extraction of extracellular vesicles (exosomes)

Exosomes are a type of nanometer-scale extracellular vesicles (EVs), which store and relay cell-specific genetic and proteomic information, thus partaking in cell communication. Exosomes can be easily and non-invasively accessed from biological fluids such as blood, urine, and saliva. However, owing to their minute sizes (30 –150 nm in diameter) and lower abundance (ranging from 0.88×10^8 to 13.38×10^8 exosomes/mL in serum or plasma [82]), there is an indispensable need for sample preparation prior to their analysis. Therefore, their extraction from biofluids is a topic of importance and interest. Yang et al. have critically analysed the techniques used for the extraction of exosomes, which include ultracentrifugation, ultrafiltration, size-exclusion chromatography, polymer precipitation, immunoaffinity capture and several

873 microfluidic approaches [83]. In addition to the advantages of cost-effectiveness and
874 high efficiency, microfluidics-based techniques allow scope for automation and facile
875 integration of exosome isolation and diagnosis at the point-of-need.

876 Some recent microfluidic advancements for separation of exosomes, for
877 example, by the use of asymmetric flow-field flow-fractionation (size-based filtration
878 by the use of a semipermeable membrane) or EOF-driven lateral displacement by using
879 nanopillar arrays, have been discussed by Berlanda et al. [84]. Both these techniques
880 leverage particle size-dependent interactions. ICP-mediated separation, on the other
881 hand is based on relative electrophoretic mobilities which is a property intrinsic and
882 unique to each analyte for a specific medium.

883 Kim et al. demonstrated ~5-fold exosome preconcentration in an origami-based
884 multi-folded μPAD device [85]. The 'accordion-shaped' device consisted of
885 convergent circular sample layers (with increasing diameters across successive layers)
886 on wax-patterned paper and Nafion®-coated layers at the two ends. The device
887 operationality involved three simple steps of sample loading, voltage application (ICP-
888 based preconcentration), and unfolding to isolate the enriched layers.

889 Cheung et al. leveraged ICP for preconcentration and trapping of EVs from
890 MDA cells, using a cation selective membrane (PEDOT:PSS) [86]. Upon the
891 application of an electric field (45 V/cm), fluorescently-labelled EVs concentrated as a
892 plug near the membrane. A highlight of the technique was the use of an ion selective
893 membrane de-coupled from the substrate used for detection – the PEDOT:PSS polymer
894 was directly printed on the PDMS channel and anchored to it by penetrating
895 micropillars. Membrane decoupling allowed flexibility in the trapping mechanism
896 either by the use of covalently modified glass substrates (superaldehyde and
897 superepoxy 3), or by using 3D-printed microtraps.

898 In another work, microfluidic gel electrophoresis was coupled with the use of an
899 ion-selective membrane in a cross-junction device to achieve electrophoretic focusing
900 and separation of exosomes from a continuously flowing sample stream on to the gel
901 matrix [87]. A sample solution containing exosomes was pumped across an intersection
902 where electrophoretic and electroosmotic forces drove exosome migration into the
903 agarose gel-filled channel. The gel matrix works to prevent larger particles such as cells
904 and debris from entering the channel. Exosomes penetrate the agarose gel pores but are
905 restricted entry into the cation-selective membrane, thereby enriching along a region at
906 the membrane interface.

These studies involve phase separation of analytes or background species (cell debris) onto substrates, traps or gel matrices. Recovery of these phases from the device or integration of on-chip analysis is a critical step towards practical implementation to clinical diagnostics.

5.6. Extraction of bioparticles (cells, organelles, viruses)

Bioparticles such as cells have a net surface charge owing to functional groups present on cell walls or membranes. In particular, gram negative bacteria such as *E.coli* have a net negative charge owing to peptidoglycan walls (with carboxyl and amino functional groups). Thus, charged bioparticles can be extracted by way of ICP. In a work by Kwak et al., continuous ICP focusing of *E.coli* was achieved using a branched flow-through device, where the concentrated analyte stream was directed towards a narrow branch of the device [67]. In another work, a high concentration (conc. factor $\sim 2 \times 10^5$) of negatively charged *E.coli* was obtained at the anodic side of a Nafion® membrane in a μPAD device [88]. Herein, a voltage bias was applied across microwire electrodes which were attached to the inlet reservoir and a band of Nafion® on the μPAD device. Preconcentration was optimized by controlling applied voltage and BGE concentration.

For bioparticles such as cells, the major challenge associated with ICP-mediated extraction is to avoid lysis. ICP has previously been leveraged to achieve bacterial cell lysis due to physicochemical changes (pH, ionic strength, temperature), vortices (shear stress) or osmotic shock [17]. These effects associated with ICP, can be detrimental for some downstream processes (e.g., cell assays) but can be mitigated by optimising voltage application, buffer and experimental conditions. Kim and co-workers protected red blood cells from vortices by creating an alternate current path through the IDZ, thereby satisfying the ionic current demanded in the overlimiting regime without the mixing provided by fluidic instabilities. To achieve this outcome, they extended the highly ionically conductive membrane outward along the microchannel floor from the ion permselective junction [89].

ICP holds promise for extraction and discrimination of smaller bioparticles including organelles and viruses. Among organelles, mitochondria have mobilities that depend upon size and membrane potential, which are characteristics impacted by aging and disease [90]. In this context, focusing could be leveraged to enrich and extract distinct subpopulations. Similarly, ICPF of virus particles has the potential to enhance

the sensitivity of viral diagnostics by facilitating purification and preconcentration prior to lateral flow assay, sensing, or viral lysis paired with nucleic acid amplification.

5.7. Extraction of non-biological particles: polystyrene particles and microbeads

Polystyrene (PS) particles can be tailor-made to suit a variety of distinct applications such as in cytometric studies, as templates in bead-based assays and as manufacturing materials. This versatility is owing, in part, to the ease with which surface functionalization, and manipulation of particle size and refractive index can be carried out [91,92]. However, being a class of microplastics, they may also render potential toxicological impacts on environment and health [93]. Their extraction is therefore an area of interest. Most commercial polystyrene particles are known to have a net negative surface charge. This property, in addition to dielectrophoretic interactions, have been utilized for their electrokinetic manipulation. The following subsections (*5.7.1–5.7.3*) discuss the implementation of radial, free-flow ICP and fICP devices for the extraction of PS particles.

5.7.1 Radial device

Lee et al. used a device with radially arranged microchannels and a circularly patterned Nafion® membrane, to focus 1-μm sized PS particles towards the central well of the device [59]. The authors reported the preconcentration of PS particles in two co-occurring forms – a compact plug and a vortical cloud shape, at the IDZ boundary. They attributed the occurrence of these two forms to the development of strong vortices within the IDZ and resultant ripples of weak vortices outside of the IDZ. Ten-fold enrichment and a recovery rate of 85.5% at the region of interest was observed.

This approach provides convenient enrichment of PS particles for subsequent analysis. To enhance enrichment, the integration of microstructuring or the employment of geometric restrictions within a radial device can be explored. In its current embodiment, the extraction approach is not continuous and is too low throughput to be practically implemented for water purification.

5.7.2 Free flow ICP

In another work, a continuous, electrophoretic mobility-based separation of polystyrene beads was reported [94]. Here, a Nafion® membrane was patterned diagonally along

the floor of the microchannel. An important point to note is that due to the angle of the membrane, an electric field component is applied normally to the flow direction along

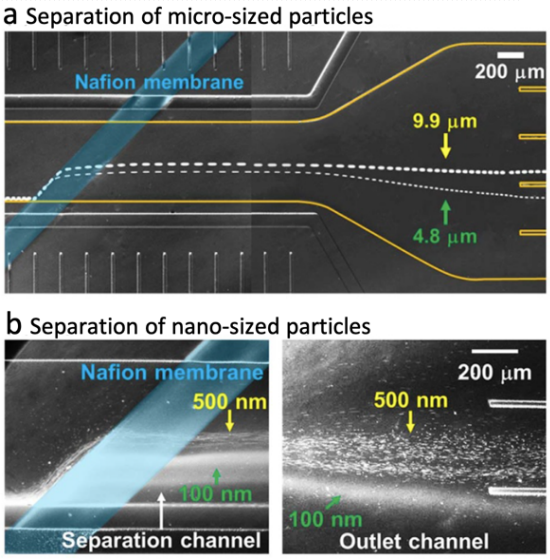

Figure 11. Micrographs showing separation of a) microsized particles having diameters 4.8 mm and 9.9 mm, and electrophoretic mobilities -4.35×10^{-4} and -6.18×10^{-4} $cm^2V^{-1}s^{-1}$ respectively and b) nanosized particles of diameters 100 nm and 500 nm, and electrophoretic mobilities -4.76×10^{-4} and -7.25×10^{-4} $cm^2V^{-1}s^{-1}$, respectively. Figure is reprinted with permission from ref [94].

the IDZ, which allowed for electrophoretic separation of particles into distinct fluid laminae (**Figure 11**). It was reported that larger-sized particles with higher electrophoretic mobilities were deflected to a greater extent from the flow field in comparison to smaller particles with lower mobilities. This finding implies that the separation is dominated by relative electrophoretic response, rather than being purely size-dependent. The authors further reported that dispersion of nanoparticles was observed to be relatively higher than that of microparticles. Dispersion was attributed to the wide range of approach paths adopted by the particles and the position of the membrane along only the bottom surface of the separation channel, which in combination, augmented the spread of exit trajectories. Therefore, the authors proposed the use of 3D flow focusing to make the particle approach to the membrane more uniform.

5.7.3 fICP and serial fICP

Crooks and coworkers leveraged fICP to facilitate ~100% redirection and separation of microplastics from BGE using a bifurcated-channel device with a split BPE [69]. The authors utilized microparticles as tracers to qualitatively map variations in EOF

generated because of fICP-induced concentration gradients and BPE response. The authors postulate that distinct rates of EOF along each of the branches of the device and the induced pressure gradient define the trajectory and effect the separation of microplastics. In subsequent work from this group, a trifurcated device was used to achieve fICP-based sorting and separation of microplastics [70]. As an initial experiment, a trifurcated-channel device was used to sort and redirect $BODIPY^{2-}$ and $\mu P1$ microparticles suspended in a BGE composed of Tris buffer. Faradaic reactions led to the formation of IDZ and IEZ. The governing mechanism of particle sorting was based on their distinct electrophoretic mobilities. Particles with higher electrophoretic mobility were deflected farther away from the IDZ, towards the region of lower electric field and into the topmost branch of the trifurcated channel. On the other hand, particles with lower electrophoretic mobilities deflected to a lower extent, towards the region of relatively higher electric field and into the middle branch. Analyte-free solution flowed through the lower-most branch. To improve focusing and separation resolution, the authors developed a serial fICP technique [70]. Herein, another set of BPEs were strategically located within the trifurcated-channel device to generate multiple electric field gradients (EFGs) within the same device and with a single power supply (**Figure 12**). The presence of two EFGs enabled redirection and streamlining of particle trajectories to decrease dispersion.

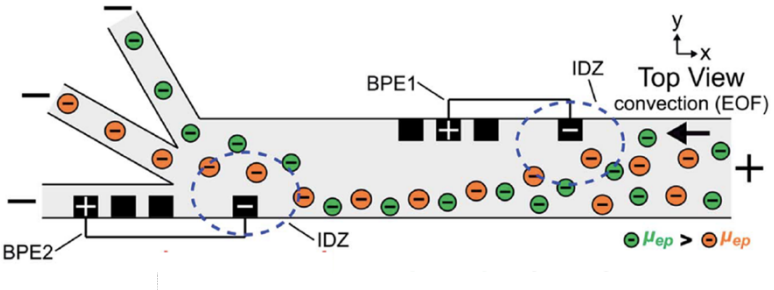

Figure 12. Device configuration, analyte transport and separation in a microfluidic device operating under serial fICP. Two sets of BPE pairs are placed at strategic locations within the device to facilitate formation of multiple electric field gradients to prefocus microplastics prior to downstream separation into distinct outlets. Figure is reprinted with permission from ref [70].

Conclusion

This review began with an introduction to ICP and provided an overview of intrinsic and extrinsic factors that impact focusing and extraction. Briefly, extrinsic factors included the applied voltage, device dimensions, architecture, placement of ion-selective membranes and electrodes, and use of auxiliary forces (e.g., pressure

modulation). Intrinsic properties such as electrophoretic mobilities of analytes, conductivity, and buffering capacity of the BGE, the nature of faradaic reactions (for fICP) and material properties of electrodes or membranes were considered. We then discussed recent advancements in ICP, highlighting instances of analyte recovery into a distinct phase and untapped opportunities for extraction.

Resolution remains a major limitation for ICP-based microextractions. For this reason, recent developments have been directed towards increasing the duration of analyte-electric field interactions either operated under orthogonal flow and electric field conditions as noted in FF-ICP [46,94] or utilized multiple EFGs, for example, in serial fICP [70]. Other approaches to improve resolution include the use of electrophoretic spacers and minimizing fluidic instabilities, for example, by microstructuring. Adding to the challenge of resolution is that the location of a focused analyte plug must be controlled to achieve its extraction into a separate phase (e.g., a solid support or a droplet), and strategies employed to steer analytes such as voltage switching, or pressure modulation worsen dispersion. Therefore, a promising area which could help circumvent the limitation of resolution and improve extraction efficiency is the integration of the extraction phase (i.e., solid phases for affinity, size exclusion, or adsorption) at the location of ICP-based enrichment or the direct extraction of analytes into pre-formed droplets.

The limited volumetric throughput of ICPF methods is a long-standing challenge, and the potential of ICPF for extraction of analytes (e.g., biopolymers), commodities (e.g., pharmaceutical products) or contaminants (e.g., microplastics) on a relevant scale remains an open question. We anticipate that this need will be met by practical approaches to stabilize fluidic vortices and to build parallel and 3D junctions for ion depletion.

An additional area for future advancement is the development of non-optical methods to monitor and quantify focusing. The reliance of ICP-based methods on fluorescence imaging drives up cost and hinders implementation ‘in the field’ or in point-of-need settings. Electrochemical methods are expected to meet this challenge; the current trace obtained at the driving electrodes during enrichment, current-voltage curves taken across the junction, electroanalysis of enriched compounds, and the integration of conductivity sensors provide a wealth of information.

Finally, for more rapid advancement of ICP-based techniques and their eventual widespread adoption, there is a pressing need for user-friendly computational tools to

predict the performance of new device designs and materials as applied to a range of sample compositions. Continual efforts via theoretical and computational studies are refining and redefining the understanding of the regimes inherent to ICP. Practical tools can be developed using approaches that decrease the computational load required to capture these multiscale (bulk to EDL) and multiphysics systems.

In conclusion, ICP-based microextractions hold immense potential for the extraction of low-abundance analytes, and for paralleled, multiphasic, on-demand or continuous extractions. The right combination of techniques, methodology and design from the palette of developments along with the wide scope for advancements in the field of ICP-based microextractions can establish new paradigms in separation sciences and associated applications.

Declaration of competing interests

The authors declare that they have no known competing financial interests or personal relationships that could have appeared to influence the work reported in this paper.

Acknowledgements

Funding for this research was provided by an NSF CAREER grant awarded by the Chemistry Directorate, Chemical Measurement and Imaging Program under award number 1849109.

References

[1] A. Wuethrich, P.R. Haddad, J.P. Quirino, The electric field - An emerging driver in sample preparation, TrAC - Trends Anal. Chem. 80 (2016) 604–611. https://doi.org/10.1016/j.trac.2016.04.016.

[2] L. Chen, X. Liu, X. Zheng, X. Zhang, J. Yang, T. Tian, Y. Liao, Dielectrophoretic separation of particles using microfluidic chip with composite three-dimensional electrode, Micromachines. 11 (2020). https://doi.org/10.3390/mi11070700.

[3] A. Alazzam, I. Stiharu, R. Bhat, A.N. Meguerditchian, Interdigitated comb-like electrodes for continuous separation of malignant cells from blood using dielectrophoresis, Electrophoresis. 32 (2011) 1327–1336. https://doi.org/10.1002/elps.201000625.

[4] C. Szydzik, K. Khoshmanesh, A. Mitchell, C. Karnutsch, Microfluidic platform for separation and extraction of plasma from whole blood using dielectrophoresis,

Biomicrofluidics. 9 (2015) 1–16. https://doi.org/10.1063/1.4938391.

[5] A. Isozaki, A. Isozaki, Y. Nakagawa, M.H. Loo, Y. Shibata, N. Tanaka, D.L. Setyaningrum, J.W. Park, Y. Shirasaki, H. Mikami, D. Huang, H. Tsoi, C.T. Riche, T. Ota, H. Miwa, Y. Kanda, T. Ito, T. Ito, K. Yamada, O. Iwata, K. Suzuki, S. Ohnuki, Y. Ohya, Y. Ohya, Y. Kato, T. Hasunuma, T. Hasunuma, S. Matsusaka, M. Yamagishi, M. Yazawa, S. Uemura, K. Nagasawa, H. Watarai, H. Watarai, D. Di Carlo, K. Goda, K. Goda, K. Goda, K. Goda, Sequentially addressable dielectrophoretic array for high-throughput sorting of large-volume biological compartments, Sci. Adv. 6 (2020) 1–12. https://doi.org/10.1126/sciadv.aba6712.

[6] K.N. Knust, E. Sheridan, R.K. Anand, R.M. Crooks, Dual-channel bipolar electrode focusing: simultaneous separation and enrichment of both anions and cations, Lab Chip. 12 (2012) 4107. https://doi.org/10.1039/c2lc40660h.

[7] R.K. Anand, E. Sheridan, K.N. Knust, R.M. Crooks, Bipolar electrode focusing: Faradaic ion concentration polarization, Anal. Chem. 83 (2011) 2351–2358. https://doi.org/10.1021/ac103302j.

[8] R. Wu, Y.P. Seah, Z. Wang, Microfluidic chip for stacking, separation and extraction of multiple DNA fragments, J. Chromatogr. A. 1437 (2016) 219–225. https://doi.org/10.1016/j.chroma.2016.01.076.

[9] F. Zarghampour, Y. Yamini, M. Baharfar, M. Faraji, Simultaneous extraction of acidic and basic drugs: Via on-chip electromembrane extraction using a single-compartment microfluidic device, Analyst. 144 (2019) 1159–1166. https://doi.org/10.1039/c8an01668b.

[10] C. Zhang, G. Sun, S. Senapati, H.C. Chang, A bifurcated continuous field-flow fractionation (BCFFF) chip for high-yield and high-throughput nucleic acid extraction and purification, Lab Chip. 19 (2019) 3853–3861. https://doi.org/10.1039/c9lc00818g.

[11] A. Ramachandran, D. Huyke, E. Sharma, M. Sahoo, N. Banaei, B. Pinsky, J. Santiago, Electric-field-driven microfluidics for rapid CRISPR-based diagnostics and its application to detection of SARS-CoV-2, (2020) 1–8. https://doi.org/10.1101/2020.05.21.109637.

[12] J.D. Spitzberg, X.F. Van Kooten, M. Bercovici, A. Meller, Microfluidic device for coupling isotachophoretic sample focusing with nanopore single-molecule sensing, Nanoscale. 12 (2020) 17805–17811. https://doi.org/10.1039/d0nr05000h.

[13] M.A. Ali, C. Hu, S. Jahan, B. Yuan, M.S. Saleh, E. Ju, S.J. Gao, R. Panat, Sensing of COVID-19 Antibodies in Seconds via Aerosol Jet Nanoprinted Reduced-Graphene-

Oxide-Coated 3D Electrodes, Adv. Mater. 2006647 (2020) 1–15. https://doi.org/10.1002/adma.202006647.

[14] Z. Yin, Z. Ramshani, J.J. Waggoner, B.A. Pinsky, S. Senapati, H.C. Chang, A non-optical multiplexed PCR diagnostic platform for serotype-specific detection of dengue virus, Sensors Actuators, B Chem. 310 (2020). https://doi.org/10.1016/j.snb.2020.127854.

[15] S. Ma, B.D. Bryson, C. Sun, S.M. Fortune, C. Lu, RNA Extraction from a Mycobacterium under Ultrahigh Electric Field Intensity in a Microfluidic Device, Anal. Chem. 88 (2016) 5053–5057. https://doi.org/10.1021/acs.analchem.6b00381.

[16] B.I. Morshed, M. Shams, T. Mussivand, Analysis of electric fields inside microchannels and single cell electrical lysis with a microfluidic device, Micromachines. 4 (2013) 243–256. https://doi.org/10.3390/mi4020243.

[17] M. Kim, L. Wu, B. Kim, D.T. Hung, J. Han, Continuous and High-Throughput Electromechanical Lysis of Bacterial Pathogens Using Ion Concentration Polarization, Anal. Chem. 90 (2018) 872–880. https://doi.org/10.1021/acs.analchem.7b03746.

[18] S. Srikanth, J.M. Mohan, S. Raut, S.K. Dubey, I. Ishii, A. Javed, S. Goel, Droplet based microfluidic device integrated with ink jet printed three electrode system for electrochemical detection of ascorbic acid, Sensors Actuators A Phys. 325 (2021) 112685. https://doi.org/10.1016/j.sna.2021.112685.

[19] C. Birch, J. Landers, Electrode Materials in Microfluidic Systems for the Processing and Separation of DNA: A Mini Review, Micromachines. 8 (2017) 76. https://doi.org/10.3390/mi8030076.

[20] D.M. Heard, A.J.J. Lennox, Electrode Materials in Modern Organic Electrochemistry, Angew. Chemie - Int. Ed. 59 (2020) 18866–18884. https://doi.org/10.1002/anie.202005745.

[21] F.C. Leinweber, U. Tallarek, Nonequilibrium electrokinetic effects in beds of ion-permselective particles, Langmuir. 20 (2004) 11637–11648. https://doi.org/10.1021/la048408n.

[22] R. Dhopeshwarkar, D. Hlushkou, M. Nguyen, U. Tallarek, R.M. Crooks, Electrokinetics in microfluidic channels containing a floating electrode, J. Am. Chem. Soc. 130 (2008) 10480–10481. https://doi.org/10.1021/ja8036405.

[23] B. Berzina, R.K. Anand, Tutorial review: Enrichment and separation of neutral and charged species by ion concentration polarization focusing, Anal. Chim. Acta. 1128 (2020) 149–173. https://doi.org/10.1016/j.aca.2020.06.021.

[24] S.J. Kim, Y.C. Wang, J.H. Lee, H. Jang, J. Han, Concentration polarization and nonlinear electrokinetic flow near a nanofluidic channel, Phys. Rev. Lett. 99 (2007) 1–4. https://doi.org/10.1103/PhysRevLett.99.044501.

[25] K. Zhou, M.L. Kovarik, S.C. Jacobson, Surface-charge induced ion depletion and sample stacking near single nanopores in microfluidic devices, J. Am. Chem. Soc. 130 (2008) 8614–8616. https://doi.org/10.1021/ja802692x.

[26] T.A. Zangle, A. Mani, J.G. Santiago, Theory and experiments of concentration polarization and ion focusing at microchannel and nanochannel interfaces, Chem. Soc. Rev. 39 (2010) 1014–1035. https://doi.org/10.1039/b902074h.

[27] M. Li, R.K. Anand, Recent advancements in ion concentration polarization, Analyst. 141 (2016) 3496–3510. https://doi.org/10.1039/C6AN00194G.

[28] K.N. Knust, E. Sheridan, R.K. Anand, R.M. Crooks, Dual-channel bipolar electrode focusing: simultaneous separation and enrichment of both anions and cations, Lab Chip. 12 (2012) 4107. https://doi.org/10.1039/c2lc40660h.

[29] W. Ouyang, X. Ye, Z. Li, J. Han, Deciphering ion concentration polarization-based electrokinetic molecular concentration at the micro-nanofluidic interface: theoretical limits and scaling laws, Nanoscale. 10 (2018) 15187–15194. https://doi.org/10.1039/c8nr02170h.

[30] V.A. Papadimitriou, L.I. Segerink, J.C.T. Eijkel, Continuous focusing, fractionation and extraction of anionic analytes in a microfluidic chip, Lab Chip. 19 (2019) 3238–3248. https://doi.org/10.1039/C9LC00434C.

[31] B. ZALTZMAN, I. RUBINSTEIN, Electro-osmotic slip and electroconvective instability, J. Fluid Mech. 579 (2007) 173–226. https://doi.org/10.1017/S0022112007004880.

[32] Y. BEN, H.-C. CHANG, Nonlinear Smoluchowski slip velocity and micro-vortex generation, J. Fluid Mech. 461 (2002) 229–238. https://doi.org/10.1017/S0022112002008662.

[33] I. Rubinstein, L. Shtilman, Voltage against current curves of cation exchange membranes, J. Chem. Soc. Faraday Trans. 2. 75 (1979) 231. https://doi.org/10.1039/f29797500231.

[34] H. Wang, V.V.R. Nandigana, K.D. Jo, N.R. Aluru, A.T. Timperman, Controlling the Ionic Current Rectification Factor of a Nanofluidic/Microfluidic Interface with Symmetric Nanocapillary Interconnects, Anal. Chem. 87 (2015) 3598–3605. https://doi.org/10.1021/ac5019638.

[35] E.V. Dydek, B. Zaltzman, I. Rubinstein, D.S. Deng, A. Mani, M.Z. Bazant, Overlimiting current in a microchannel, Phys. Rev. Lett. 107 (2011) 1–5. https://doi.org/10.1103/PhysRevLett.107.118301.

[36] K. Kim, W. Kim, H. Lee, S.J. Kim, Stabilization of ion concentration polarization layer using micro fin structure for high-throughput applications, Nanoscale. 9 (2017) 3466–3475. https://doi.org/10.1039/C6NR08978J.

[37] J. Kim, I. Cho, H. Lee, S.J. Kim, Ion Concentration Polarization by Bifurcated Current Path, Sci. Rep. 7 (2017) 1–12. https://doi.org/10.1038/s41598-017-04646-0.

[38] J. De Valença, M. Jõgi, R.M. Wagterveld, E. Karatay, J.A. Wood, R.G.H. Lammertink, Confined Electroconvective Vortices at Structured Ion Exchange Membranes, Langmuir. 34 (2018) 2455–2463. https://doi.org/10.1021/acs.langmuir.7b04135.

[39] B. Berzina, S. Kim, U. Peramune, K. Saurabh, B. Ganapathysubramanian, R.K. Anand, Out-of-plane faradaic ion concentration polarization: stable focusing of charged analytes at a three-dimensional porous electrode, Lab Chip. (2022) 1037–1043. https://doi.org/10.1039/D1LC01011E.

[40] Y. Ding, P.D. Howes, A.J. Demello, Recent advances in droplet microfluidics, Anal. Chem. 92 (2020) 132–149. https://doi.org/10.1021/acs.analchem.9b05047.

[41] M. Tenje, A. Fornell, M. Ohlin, J. Nilsson, Particle Manipulation Methods in Droplet Microfluidics, Anal. Chem. 90 (2018) 1434–1443. https://doi.org/10.1021/acs.analchem.7b01333.

[42] S. Kim, B. Ganapathysubramanian, R.K. Anand, Concentration Enrichment, Separation, and Cation Exchange in Nanoliter-Scale Water-in-Oil Droplets, J. Am. Chem. Soc. 142 (2020) 3196–3204. https://doi.org/10.1021/jacs.9b13268.

[43] D.T. Phan, Y. Chun, N.T. Nguyen, A continuous-flow droplet-based concentrator using ion concentration polarization, RSC Adv. 5 (2015) 44336–44341. https://doi.org/10.1039/c5ra07491f.

[44] V.A. Papadimitriou, S.A. Kruit, L.I. Segerink, J.C.T. Eijkel, Droplet encapsulation of electrokinetically-focused analytes without loss of resolution, Lab Chip. 20 (2020) 2209–2217. https://doi.org/10.1039/D0LC00191K.

[45] L. Gong, W. Ouyang, Z. Li, J. Han, Direct numerical simulation of continuous lithium extraction from high Mg2+/Li+ ratio brines using microfluidic channels with ion concentration polarization, J. Memb. Sci. 556 (2018) 34–41. https://doi.org/10.1016/j.memsci.2018.03.078.

[46] V.A. Papadimitriou, L.I. Segerink, J.C.T. Eijkel, Free Flow Ion Concentration Polarization Focusing (FF-ICPF), Anal. Chem. 92 (2020) 4866–4874. https://doi.org/10.1021/acs.analchem.9b04526.

[47] J. Choi, K. Huh, D.J. Moon, H. Lee, S.Y. Son, K. Kim, H.C. Kim, J.-H. Chae, G.Y. Sung, H.-Y. Kim, J.W. Hong, S.J. Kim, Selective preconcentration and online collection of charged molecules using ion concentration polarization, RSC Adv. 5 (2015) 66178–66184. https://doi.org/10.1039/C5RA12639H.

[48] M.S. Sotoudegan, O. Mohd, F.S. Ligler, G.M. Walker, Paper-based passive pumps to generate controllable whole blood flow through microfluidic devices, Lab Chip. 19 (2019) 3787–3795. https://doi.org/10.1039/C9LC00822E.

[49] T. Ozer, C. Mcmahon, C.S. Henry, Annual Review of Analytical Chemistry Advances in Paper-Based Analytical Devices, Annu. Rev. Anal. Chem. 13 (2020) 4.1-4.25. https://doi.org/10.1146/annurev-anchem-061318-.

[50] L.M. Fu, Y.N. Wang, Detection methods and applications of microfluidic paper-based analytical devices, TrAC - Trends Anal. Chem. 107 (2018) 196–211. https://doi.org/10.1016/j.trac.2018.08.018.

[51] K. Lee, Y.K. Yoo, S. Il Han, J. Lee, D. Lee, C. Kim, J.H. Lee, Folding-paper-based preconcentrator for low dispersion of preconcentration plug, Micro Nano Syst. Lett. 5 (2017) 11. https://doi.org/10.1186/s40486-017-0045-y.

[52] A. Zargaryan, N. Farhoudi, G. Haworth, J.F. Ashby, S.H. Au, Hybrid 3D printed-paper microfluidics, Sci. Rep. 10 (2020) 18379. https://doi.org/10.1038/s41598-020-75489-5.

[53] S. Terabe, Micellar electrokinetic chromatography for high-performance analytical separation, Chem. Rec. 8 (2008) 291–301. https://doi.org/10.1002/tcr.20156.

[54] B. Berzina, R.K. Anand, An Electrokinetic Separation Route to Source Dialysate from Excess Fluid in Blood, Anal. Chem. 90 (2018) 3720–3726. https://doi.org/10.1021/acs.analchem.7b02584.

[55] B. Berzina, R.K. Anand, Continuous micellar electrokinetic focusing of neutral species driven by ion concentration polarization, Lab Chip. 19 (2019) 2233–2240. https://doi.org/10.1039/c9lc00327d.

[56] S. Li, C. Zhang, S. Wang, Q. Liu, H. Feng, X. Ma, J. Guo, Electrochemical microfluidics techniques for heavy metal ion detection, Analyst. 143 (2018) 4230–4246. https://doi.org/10.1039/c8an01067f.

[57] S.A. Jaywant, K. Mahmood Arif, A comprehensive review of micro fluidic water

quality monitoring sensors, Sensors (Switzerland). 19 (2019). https://doi.org/10.3390/s19214781.

[58] V. Subramanian, S. Lee, S. Jena, S.K. Jana, D. Ray, S.J. Kim, P. Thalappil, Enhancing the sensitivity of point-of-use electrochemical microfluidic sensors by ion concentration polarisation – A case study on arsenic, Sensors Actuators, B Chem. 304 (2020) 127340. https://doi.org/10.1016/j.snb.2019.127340.

[59] S. Lee, S. Park, W. Kim, S. Moon, H.Y. Kim, H. Lee, S.J. Kim, Nanoelectrokinetic bufferchannel-less radial preconcentrator and online extractor by tunable ion depletion layer, Biomicrofluidics. 13 (2019) 1–12. https://doi.org/10.1063/1.5092789.

[60] D.T. Chiu, A.J. deMello, D. Di Carlo, P.S. Doyle, C. Hansen, R.M. Maceiczyk, R.C.R. Wootton, Small but Perfectly Formed? Successes, Challenges, and Opportunities for Microfluidics in the Chemical and Biological Sciences, Chem. 2 (2017) 201–223. https://doi.org/10.1016/j.chempr.2017.01.009.

[61] F.A. Vicente, I. Plazl, S.P.M. Ventura, P. Žnidaršič-Plazl, Separation and purification of biomacromolecules based on microfluidics, Green Chem. 22 (2020) 4391–4410. https://doi.org/10.1039/c9gc04362d.

[62] W. Hellmich, J. Regtmeier, T.T. Duong, R. Ros, D. Anselmetti, A. Ros, Poly(oxyethylene) based surface coatings for poly(dimethylsiloxane) microchannels, Langmuir. 21 (2005) 7551–7557. https://doi.org/10.1021/la0510432.

[63] E.A.S. Doherty, R.J. Meagher, M.N. Albarghouthi, A.E. Barron, Microchannel wall coatings for protein separations by capillary and chip electrophoresis, Electrophoresis. 24 (2003) 34–54. https://doi.org/10.1002/elps.200390029.

[64] S.A. Hong, Y.-J. Kim, S.J. Kim, S. Yang, Electrochemical detection of methylated DNA on a microfluidic chip with nanoelectrokinetic pre-concentration, Biosens. Bioelectron. 107 (2018) 103–110. https://doi.org/10.1016/j.bios.2018.01.067.

[65] B. Lu, M.M. Maharbiz, Ion concentration polarization (ICP) of proteins at silicon micropillar nanogaps, PLoS One. 14 (2019) 1–17. https://doi.org/10.1371/journal.pone.0223732.

[66] B. Sabbagh, E. Stolovicki, S. Park, D.A. Weitz, G. Yossifon, Tunable Nanochannels Connected in Series for Dynamic Control of Multiple Concentration-Polarization Layers and Preconcentrated Molecule Plugs, Nano Lett. 20 (2020) 8524–8533. https://doi.org/10.1021/acs.nanolett.0c02973.

[67] R. Kwak, S.J. Kim, J. Han, Continuous-Flow Biomolecule and Cell Concentrator by Ion Concentration Polarization, Anal. Chem. 83 (2011) 7348–7355.

https://doi.org/10.1021/ac2012619.
[68] D.T. Phan, L. Jin, S. Wustoni, C.H. Chen, Buffer-free integrative nanofluidic device for real-time continuous flow bioassays by ion concentration polarization, Lab Chip. 18 (2018) 574–584. https://doi.org/10.1039/c7lc01066d.
[69] C.D. Davies, E. Yoon, R.M. Crooks, Continuous Redirection and Separation of Microbeads by Faradaic Ion Concentration Polarization, ChemElectroChem. 5 (2018) 877–884. https://doi.org/10.1002/celc.201700450.
[70] C.D. Davies, R.M. Crooks, Focusing, sorting, and separating microplastics by serial faradaic ion concentration polarization, Chem. Sci. 11 (2020) 5547–5558. https://doi.org/10.1039/D0SC01931C.
[71] W. Ouyang, J. Han, Universal amplification-free molecular diagnostics by billion-fold hierarchical nanofluidic concentration, Proc. Natl. Acad. Sci. U. S. A. 116 (2019) 16240–16249. https://doi.org/10.1073/pnas.1904513116.
[72] B. Scarff, C. Escobedo, D. Sinton, Radial sample preconcentration, Lab Chip. 11 (2011) 1102–1109. https://doi.org/10.1039/c0lc00326c.
[73] C.H. Chen, A. Sarkar, Y.A. Song, M.A. Miller, S.J. Kim, L.G. Griffith, D.A. Lauffenburger, J. Han, Enhancing protease activity assay in droplet-based microfluidics using a biomolecule concentrator, J. Am. Chem. Soc. 133 (2011) 10368–10371. https://doi.org/10.1021/ja2036628.
[74] M.A. Saucedo-Espinosa, P.S. Dittrich, In-Droplet Electrophoretic Separation and Enrichment of Biomolecules, Anal. Chem. 92 (2020) 8414–8421. https://doi.org/10.1021/acs.analchem.0c01044.
[75] M.M. Gong, R. Nosrati, M.C. San Gabriel, A. Zini, D. Sinton, Direct DNA Analysis with Paper-Based Ion Concentration Polarization, J. Am. Chem. Soc. 137 (2015) 13913–13919. https://doi.org/10.1021/jacs.5b08523.
[76] X. Li, L. Luo, R.M. Crooks, Faradaic Ion Concentration Polarization on a Paper Fluidic Platform, Anal. Chem. 89 (2017) 4294–4300. https://doi.org/10.1021/acs.analchem.7b00365.
[77] S.H. Yeh, K.H. Chou, R.J. Yang, Sample pre-concentration with high enrichment factors at a fixed location in paper-based microfluidic devices, Lab Chip. 16 (2016) 925–931. https://doi.org/10.1039/c5lc01365h.
[78] Y.-Z. Chen, B.-S. Niu, B. Ji, F. Fang, X.-L. Guo, Z.-Y. Wu, Salty Biofluidic Sample Clean-Up and Preconcentration with a Paper-Based Ion Concentration Polarization Interface, Anal. Chem. 93 (2021) 10236–10242.

https://doi.org/10.1021/acs.analchem.1c01640.
[79] H. Gao, J.J. Liu, Y.Q. Liu, Z.Y. Wu, Detection of urine protein by a paper-based analytical device enhanced with ion concentration polarization effect, Microfluid. Nanofluidics. 23 (2019) 1–7. https://doi.org/10.1007/s10404-019-2220-3.
[80] S. Il Han, Y.K. Yoo, J. Lee, C. Kim, K. Lee, T.H. Lee, H. Kim, D.S. Yoon, K.S. Hwang, R. Kwak, J.H. Lee, High-ionic-strength pre-concentration via ion concentration polarization for blood-based biofluids, Sensors Actuators, B Chem. 268 (2018) 485–493. https://doi.org/10.1016/j.snb.2018.04.144.
[81] J. Lee, Y.K. Yoo, D. Lee, C. Kim, K.H. Kim, S. Lee, S. Kwak, J.Y. Kang, H. Kim, D.S. Yoon, D. Hur, J.H. Lee, Origami paper-based sample preconcentration using sequentially driven ion concentration polarization, Lab Chip. 21 (2021) 867–874. https://doi.org/10.1039/D0LC01032D.
[82] E.R. Sauter, Exosomes in blood and cancer, Transl. Cancer Res. 6 (2017) S1316–S1320. https://doi.org/10.21037/tcr.2017.08.13.
[83] D. Yang, W. Zhang, H. Zhang, F. Zhang, L. Chen, L. Ma, L.M. Larcher, S. Chen, N. Liu, Q. Zhao, P.H.L. Tran, C. Chen, R.N. Veedu, T. Wang, Progress, opportunity, and perspective on exosome isolation - Efforts for efficient exosome-based theranostics, Theranostics. 10 (2020) 3684–3707. https://doi.org/10.7150/thno.41580.
[84] S.F. Berlanda, M. Breitfeld, C.L. Dietsche, P.S. Dittrich, Recent Advances in Microfluidic Technology for Bioanalysis and Diagnostics, Anal. Chem. 93 (2021) 311–331. https://doi.org/10.1021/acs.analchem.0c04366.
[85] H. Kim, K.H. Lee, S. Il Han, D. Lee, S. Chung, D. Lee, J.H. Lee, Origami-paper-based device for microvesicle/exosome preconcentration and isolation, Lab Chip. 19 (2019) 3917–3921. https://doi.org/10.1039/c9lc00796b.
[86] L.S. Cheung, S. Sahloul, A. Orozaliev, Y.A. Song, Rapid detection and trapping of extracellular vesicles by electrokinetic concentration for liquid biopsy on chip, Micromachines. 9 (2018). https://doi.org/10.3390/mi9060306.
[87] S. Marczak, K. Richards, Z. Ramshani, E. Smith, S. Senapati, R. Hill, D.B. Go, H.C. Chang, Simultaneous isolation and preconcentration of exosomes by ion concentration polarization, Electrophoresis. 39 (2018) 2029–2038. https://doi.org/10.1002/elps.201700491.
[88] A.T.K. Perera, S. Pudasaini, S.S.U. Ahmed, D.T. Phan, Y. Liu, C. Yang, Rapid pre-concentration of Escherichia coli in a microfluidic paper-based device using ion concentration polarization, Electrophoresis. 41 (2020) 867–874.

https://doi.org/10.1002/elps.201900303.
[89] J. Kim, I. Cho, H. Lee, S.J. Kim, Ion Concentration Polarization by Bifurcated Current Path, Sci. Rep. 7 (2017) 5091. https://doi.org/10.1038/s41598-017-04646-0.
[90] G.G. Wolken, E.A. Arriaga, Simultaneous Measurement of Individual Mitochondrial Membrane Potential and Electrophoretic Mobility by Capillary Electrophoresis, Anal. Chem. 86 (2014) 4217–4226. https://doi.org/10.1021/ac403849x.
[91] I. Bangs Laboratories, Working with Microspheres, Bangs Lab. (2013) 1–16. papers3://publication/uuid/C97A145C-472E-40F9-BAB6-9FF93E44BE5B.
[92] D. Sarma, P. Carl, E. Climent, R.J. Schneider, K. Rurack, Multifunctional Polystyrene Core/Silica Shell Microparticles with Antifouling Properties for Bead-Based Multiplexed and Quantitative Analysis, ACS Appl. Mater. Interfaces. 11 (2019) 1321–1334. https://doi.org/10.1021/acsami.8b10306.
[93] J. Hwang, D. Choi, S. Han, S.Y. Jung, J. Choi, J. Hong, Potential toxicity of polystyrene microplastic particles, Sci. Rep. 10 (2020) 1–12. https://doi.org/10.1038/s41598-020-64464-9.
[94] H. Jeon, H. Lee, K.H. Kang, G. Lim, Ion concentration polarization-based continuous separation device using electrical repulsion in the depletion region, Sci. Rep. 3 (2013) 1–7. https://doi.org/10.1038/srep03483.